sciendo
Austrian Journal of Earth Sciences | Vienna | 2018 | Volume 111/1 | 135 - 154 | DOI: 10.17738/ajes.2018.0009

Palynology of the Cenomanian Raha Formation, Gulf of Suez, Egypt: Biostratigraphical, palaeoenvironmental and palaeobiogeographical implications

Omar MOHAMED[1)*)], Ahmed MANSOUR[1)], Sameh S. TAHOUN[2)], Ashraf M. T. ELEWA[1)] & Muhammad Ali MEKKEY[3)]

[1)] Geology Department, Faculty of Science, Minia University, P.O. Box 61519, Minia, Egypt;

[2)] Geology Department, Faculty of Science, Cairo University, P.O. Box 12613, Giza, Egypt;

[3)] West Bakr Petroleum Company, P.O. Box 546 Cairo-code No. 11371, Nasr City, Cairo, Egypt;

[*)] Corresponding author: omar.mohamed@mu.edu.eg

KEYWORDS Cenomanian; palynostratigraphy; palaeoenvironment; palaeobiogeography; palynofacies; Gulf of Suez

Abstract

The current study presents a fully qualitative palynological investigation carried out on the Raha Formation encountered from three wells in the Bakr Oil Field of the Gulf of Suez, Egypt. Around 30 species of pteridophytic spores, 26 species of angiosperm pollen, 24 species of gymnosperm pollen and 27 species of dinoflagellate cysts have been recorded. However, achritarchs, microforaminiferal test linings and freshwater algae are impoverished and sparsely documented throughout the Raha Formation. Two palynozones have been identified based on some stratigraphically significant pollen and spores, arranged from youngest to oldest: (1) Palynozone I (*Classopollis brasiliensis–Tricolpites sagax* Assemblage Zone) of late Cenomanian age; (2) Palynozone II (*Afropollis jardinus–Crybelosporites pannuceus* Assemblage Zone) of early-middle Cenomanian age. The distribution and ecological affiliation of specific palynomorph species, as well as various palynofacies parameters, are interpreted. A shallow marine environment from supratidal to distal inner neritic under proximal suboxic–anoxic to dysoxic–anoxic shelf conditions is reconstructed. Palaeobiogeographically, the absence of elaters from the recovered taxa is interpreted in terms of minor floral variation. This may be attributed to climatic and/or an environment-controlled niche establishment, which possibly was shaped by the existence of a physical barrier hindering the distribution of such type of elaterate parent plants.

1. Introduction

Cenomanian deposits of the Tethyan region are widespread in Egypt and in neighbouring countries, for instance, Libya (e.g. Batten and Uwins, 1985; Thusu et al., 1988), Sudan (e.g. Schrank and Awad, 1990; Schrank, 1992, 1994), Nigeria (e.g. Lawal and Moullade, 1986), and northern Europe. During this time interval, the Neo-Tethyan transgression event inundated the cratonic areas in northern and central parts of Egypt (El Beialy et al., 2010, 2011; Tahoun and Deaf, 2016; Mansour et al., 2018), North-Central Spain (Floquet, 1998; Peyrot et al., 2011), the Czech Republic (Čech, 2005) and northern Europe (Olde et al., 2015), mainly driven by tectonic forces and eustasy (Haq, 2014).

Various palynological studies on Cretaceous sediments have been carried out all over the Tethyan territory, especially concentrating on the Cenomanian–Turonian boundary interval, which includes one of the most severe oxygen-deficiency crises in the Mesozoic, i.e. Oceanic Anoxic Event (OAE) 2 (Schlanger et al., 1987), also known in Austria (e.g. Pavlishina and Wagreich, 2012).

The Cenomanian deposits in Egypt are recorded from the Eastern and Western Deserts. The present study aims to differentiate between the early-middle and late Cenomanian ages of the Raha Formation through palynological and biostratigraphical analysis. In addition, we try to interpret the palaeoenvironmental conditions based on quantitative and qualitative palynological data. The studied samples of the Raha Formation have been taken from the Bakr Oil Field (BOF) in the Gulf of Suez, which is one of the most prolific oil provinces in Egypt (Egyptian General Petroleum Corporation [EGPC], 1996). The Cenomanian Raha Formation is one of the promising intervals in the Gulf of Suez region due to its mostly clastic composition.

Previous palynological studies on the Cenomanian successions in Egypt have been carried out mostly in the northern region of the Western Desert (e.g. Aboul Ela and Mahrous, 1992; El Shamma and Arafa, 1992; Schrank and Ibrahim, 1995; Mahmoud and Moawad, 2000; El Beialy et al., 2010, 2011; Tahoun, 2012; Tahoun and Mohamed, 2013; Tahoun et al., 2013, 2015; Tahoun and Deaf, 2016). On the other hand, those that have focussed on the Cretaceous period of the Gulf of Suez include only the study by Mahmoud et al. (2007).

2. Geologic setting

The Gulf of Suez covers an area of about 25,000 km^2 and extends from latitudes 27°30′ N to 30°00′ N (Fig. 1). It runs in a northwest–southeast direction and forms an elongated graben with a length of about 320 km. The Gulf of Suez formed as the northern extension of the Red Sea rifting event. The Gulf rift was attributed to be initiated possibly by two main dynamic forces: regional

Figure 1: Geological map of the study area within the Gulf of Suez region (modified after Alsharhan, 2003); the inset figure shows the location of the three wells under study.

extension across shear zones and/or by the right–lateral coupled force along it (Meshref, 1990). Rifting occurred during the repeated lateral displacement between the Arabian Plate and the Sinai Peninsula in the Late Eocene–Oligocene epochs (EGPC, 1996). However, Boukhary et al. (2012) stated that the rifting event occurred during the latest Oligocene–Early Miocene period. Therefore, the main structural elements of this rift are half grabens. On the other hand, the Gulf Rift is subdivided into three main provinces based on the structural dip of the sedimentary cover (Moustafa, 1976): the northern Wadi Araba, central Belayim and the southern Aml provinces, separated by the Galala–Abu Zenima and Morgan Hinge zones, respectively (Bosworth and McClay, 2001).

The BOF is located in the central Belayim province. It consists primarily of two structurally horst blocks. The southwest block displays a N–NW trend, whereas the second one trends more to the NW (EGPC, 1996). Furthermore, Bosworth and McClay (2001) presumed that the central province of the Gulf commenced rifting from approximately 25–23 Ma onwards.

In the present study, a normal fault cut across the three wells, throwing down to the west of Bakr Main Basin (Fig. 2). As a result, the absence of Palynozone I (late Cenomanian) is attributed mainly to faulting and erosion of the upper part of the Raha Formation in B-115 (Fig. 2). Therefore, the structure indirectly influences the distribution and the lateral variation of palynozone thicknesses. Additional structural data of the Bakr-81 well have been used to improve the subsurface structure between B-109 and B-115.

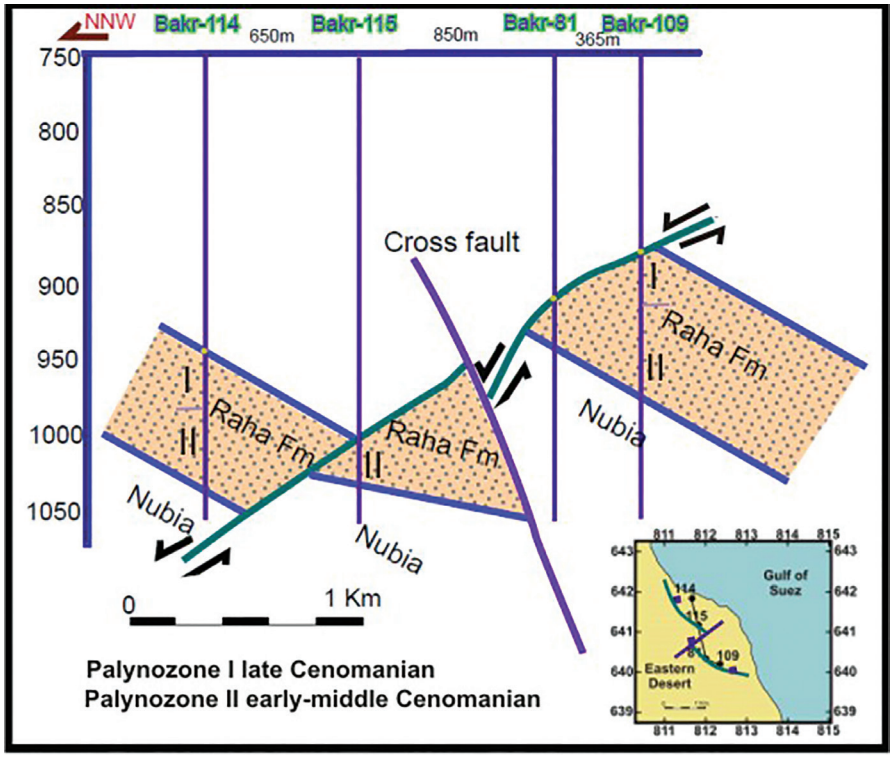

Figure 2: Geologic cross-section with major structural features through the Bakr Oil Field with the encountered wells.

3. Lithostratigraphy

The lithostratigraphic succession of the BOF ranges in age from the Precambrian to the Holocene (EGPC, 1996) and has been subdivided basically into three groups relative to the Miocene rifting event as follows: the pre-rift succession (Pre-Cambrian basement to the upper Eocene); the syn-rift succession (Oligocene–Miocene) and the post-rift succession (post-Miocene). The present study concentrates on the Raha Formation, which belongs to the pre-rift stage.

The Raha Formation was defined by Ghorab (1961) and is composed, at its type locality (Gebel Raha, western Sinai), of a 70- to 120-m-thick clastic and carbonate succession. The three studied intervals of the Raha Formation primarily consist of alternating grey-to-black shale and limestone, with minor intercalations of sandstone. It is overlain by the Abu Qada Formation and unconformably underlain by the Nubia A Formation. The Raha Formation was dated biostratigraphically to be Cenomanian in age (Ghorab, 1961; Abdallah and El-Adindani, 1963; Kora et al., 1994). The Raha Formation is equivalent to the Galala Formation described by Awad and Abdallah (1966) in the northern region of the Eastern Desert (Northern and Southern Galala plateaus). The vertical drilling thicknesses of the Raha Formation measured 100, 94 and 34 m in wells B-109, B-114 and B-115, respectively.

4. Materials and methods

The selected material for the present study was obtained from the General Petroleum Company (GPC) in Egypt. A total of 60 cutting samples with their composite logs from three boreholes in the BOF in the western coast of the Gulf of Suez have been palynologically investigated. The first well named B-114 was drilled by the GPC during 2003, at 28°28′07.26″N and 33°00′28.61″E, whereas B-115, was drilled during 2004, at 28°27′43.86″N and 33°00′33.95″E. The third well, B-109, was drilled by the GPC during 2001, at 28°27′13.25″N and 33°00′53.58″E.

All samples were processed using standard palynological preparation techniques (e.g. Wood et al., 1996). Each sample (15 g) was treated with concentrated HF and HCl acids and then sieved using a nylon screen with a mesh size of 15 µm. No oxidative agents (e.g. hydroxides, nitric acid and ultrasonic treatment) were used. Canada balsam was used as the mounting medium for two microscope slides after extensive mixing to obtain homogeneity and covered by a slide cover (20 × 40 mm).

All slides and residues are stored in the Micropalaeontology and Stratigraphy Laboratory at the Faculty of Science, Minia University, Egypt.

According to Tyson (1995), the ideal count is >500 particles per sample. In the present work, a total of 1,000 particles per sample were counted (Supplementary data: Tables 1–3), as well as the counts of palynofacies categories (Supplementary data: Tables 4–6).

5. Results and discussion

The preservation of palynomorphs within the studied samples from the BOF is fair to good. The majority of samples are dominated by amorphous organic matter (AOM) and phytoclasts (black and translucent debris), with a low content of palynomorphs, mainly sporomorphs. Dinoflagellate cysts and acritarchs have low to rare occurrence, respectively. In general, the palynomorph percentages do not exceed 19.6% of the total organic matter yield throughout the studied intervals. Individual spore and pollen specimens often exhibit signs of post-depositional degradation and distortion. However, the diversity pattern may ultimately be influenced by differential unfavourable conditions of preservation of palynomorphs (Schrank, 2003). In the same context, the dinoflagellate cysts, being badly preserved, display a pronounced surface degradation, which can be observed in carbonate rocks, due to their alkaline properties (Schrank, 1988). Dinoflagellate cyst diversity is very low throughout the three boreholes, mostly represented by one or two specimens per sample. All counted samples are plotted in the AOM-Phytoclasts-Palynomorphs ternary diagram after Tyson (1995) (Fig. 3).

5.1. Palynostratigraphy and age assessment

An assemblage of 124 palynomorph species belonging to 77 genera was defined from the examined samples. Two palynozones have been established based upon the first downhole occurrence of the recorded marker taxa and the relative abundance data. Most of the palynomorph taxa, identified in the present study, are presented in the semi-quantitative distribution range charts (Fig. 4). The well preserved taxa and the taxa of stratigraphic significance are illustrated in Figures 5 and 6. The present work deals predominantly with the miospore record; however, the biostratigraphic significance of some dinocyst species is also discussed. The established assemblages could be correlated with their equivalents in the Gulf of Suez and the Western Desert, as well as outside Egypt. Two palynological biozones from the youngest to the oldest are discussed.

5.1.1. Palynozone I *Classopollis brasiliensis–Tricolpites sagax* Assemblage Zone

Zone definition

This zone is defined by the first downhole occurrence of *C. brasiliensis* and *T. sagax*, and it extends downwards to the first downhole occurrence of *Afropollis jardinus* or *Crybelosporites pannuceus.*

Occurrence

In B-114, this zone occurred from depth of 987 m to 945 m (42-m thickness) of the Raha Formation, while in B-109, it was found from 915 m to 876 m depth (28 m thick) (Fig. 4).

Diagnosis

Apart from the aforementioned marker species of this zone, other important taxa, such as *Nyssapollenites* spp., *Balmeiopsis limbatus*, *Triporites* spp. and *Foveotricolpites* spp., were recorded (Figs. 4 and 5).

Associated taxa

Exesipollenites spp., *Monocolpopollenites* spp., *Classopollis torosus*, *Araucariacites australis*, *A. hungaricus*, *Inaperturopollenites* spp., *Spheripollenites* spp., *Arecipites* spp., *Exochosphaeridium bifidum*, *Coronifera oceanica* and *Trichodinium castanea* were reported in Palynozone I (Figs. 4 and 5).

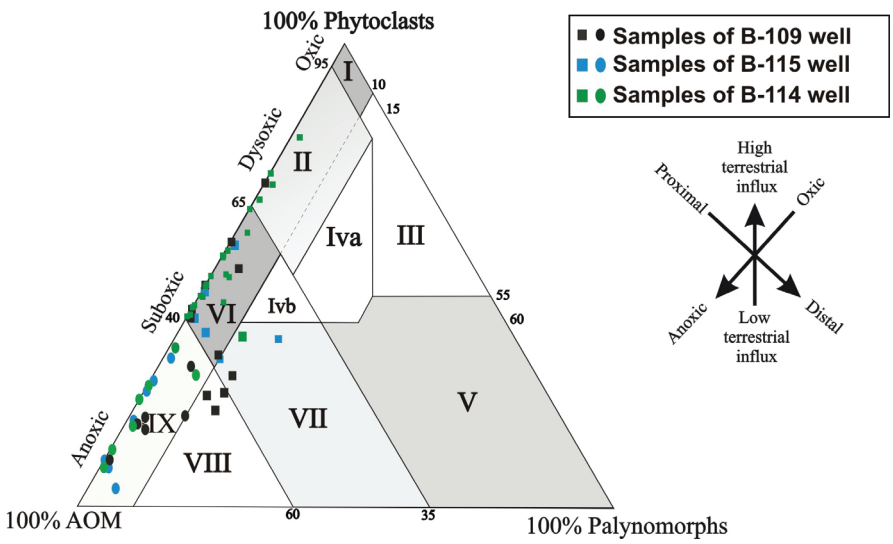

Figure 3: AOM-Palynomorphs-Phytoclasts ternary diagram (after Tyson, 1995) of samples in Bakr-114, Bakr-109 and Bakr-115 wells, Bakr Oil Field, Gulf of Suez Basin.

Proposed age

The presumed age is late Cenomanian.

Correlation

The present Palynozone I can be correlated with the VII and VIII zones in West Africa (Jardiné and Magloire, 1965) and the upper part of the II and III zones of the Cenomanian succession from 1-QS-1-MA well in the State of Maranhao, Brazil (Herngreen, 1973). Moreover, Lawal and Moullade (1986) documented *Classopollis brasiliensis* and *Triorites africaensis* of a late Cenomanian age in the upper part of Zones I (Subzone Ib) and II of the sediments in the Upper Benue Basin, Northeastern Nigeria (Fig. 7). However, the geographical

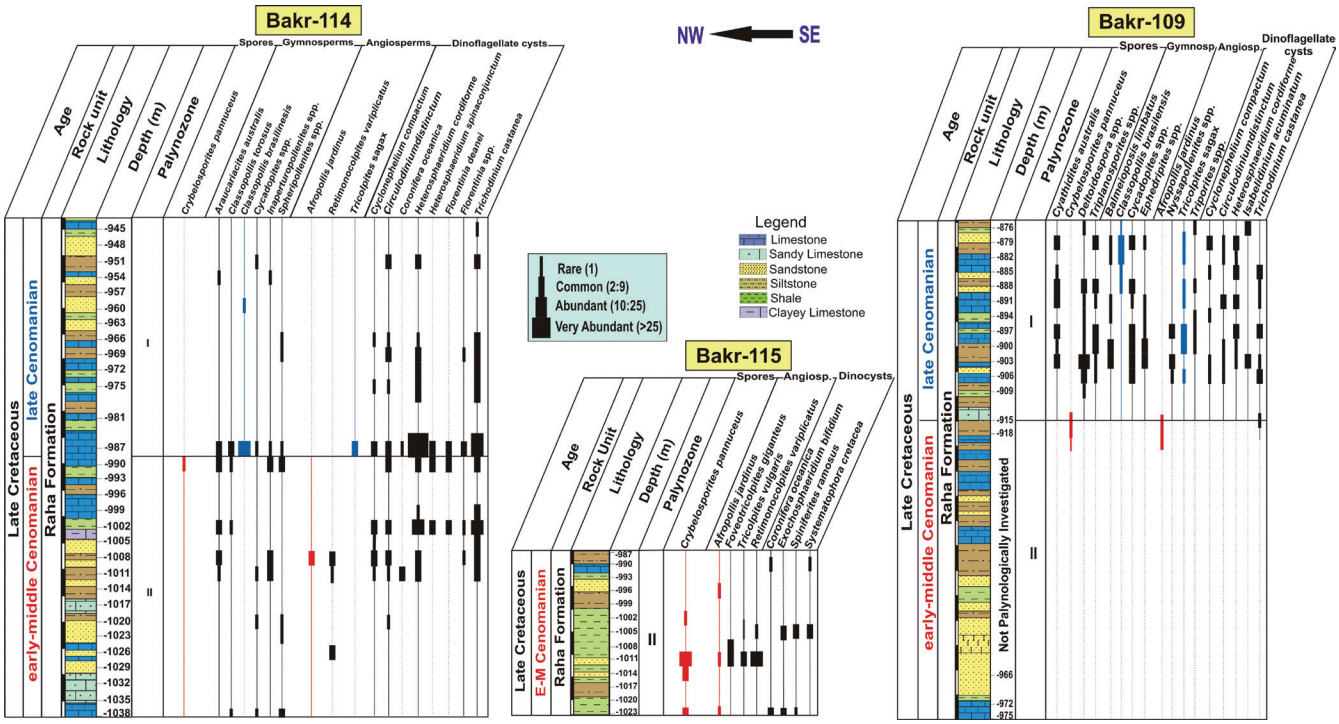

Figure 4: Range chart of selected palynomorphs taxa in B-114, B-115 and B-109 wells.

distribution of the marker species *Triorites africaensis* is not included herein and it is absent in the Gulf of Suez region. Consequently, Thusu et al. (1988) documented the last appearance datum of *C. brasiliensis* as in the late Cenomanian of the Northeast of Libya (Fig. 7).

In the Cenomanian microfloristic province of the northern parts of the Western Desert of Egypt, *C. brasiliensis* was documented from a subsurface palynologically dated as belonging to the late Cenomanian sequence (e.g. Aboul Ela and Mahrous, 1992; El Shamma and Arafa, 1992; Schrank and Ibrahim, 1995; Mahmoud and Moawad, 2000). Recently, El Beialy et al. (2011) assumed an age as young as late Cenomanian for the basal part of the Abu Roash Formation, based on the predominance of the herein-recorded *C. brasiliensis* along with *Afropollis* cf. *kahramanensis* and *Dichastopollenites ghazalataensis* in the northern part of the Western Desert of Egypt. Nevertheless, *A.* cf. *kahramanensis* and *D. ghazalataensis* are not documented in the current study. In addition, Tahoun (2012) and Tahoun and Deaf (2016) identified the same gymnosperm marker taxon *C. brasiliensis* and presumed a late Cenomanian age for the Abu Roash "G" Member from the Abu Gharadig Basin and Matruh Basin in the extreme northern region of the Western Desert, Egypt, respectively.

The last appearance of *T. sagax* has been recorded from the upper Cenomanian strata of Abu Gharadig Basin in the northern part of the Western Desert of Egypt (El-Beialy, 1994 a, b). Moreover, Schrank and Awad (1990) identified the same species within the upper Cenomanian strata of Khartoum area, Sudan. Srivastava (1994) reported *T. sagax* from an upper Cenomanian interval in the Southern Coastal areas of Tanzania. Nevertheless, such an angiosperm species has also been widely documented from the Huincul Formation in the Neuquén Basin, Argentina (Vallati, 2001), France (Azéma et al., 1972; Ducreux and Gaillard, 1986) and Canada (Burden and Langille, 1991). *Tricolpites* cf. *sagax* and *Araucariacites australis* have been recorded from the upper Cenomanian strata in the Bohemian Cretaceous Basin, Czech Republic (Čech et al., 2005).

The *Triporites* pollen species is recorded within Palynozone I and is considered as significant marker species. Its appearance is generally reported from the upper Cenomanian of the Northern Gondwana Realm (Jardiné and Magloire, 1965; Herngreen, 1973, 1975; Boltenhagen, 1980; Lawal and Moullade, 1986; Muller et al., 1987; Regali 1989; Salard-Cheboldaeff 1990). In Sudan, Schrank (1992, 1994) documented *Triporites* pollen species from the upper Cenomanian strata of northern Kordofan. In Egypt, Schrank and Ibrahim (1995) recorded its occurrence in the upper Cenomanian deposits of Northwestern Egypt. Moreover, Ibrahim (1996) identified *Triporites* sp. from an upper Cenomanian succession from Ghazalat-1 Well in Qattara Depression, Western Desert, Egypt.

Davey and Verdier (1973) recorded *Florentinia deanei* and other *Florentinia* species in the Tethyan Realm. Deflandre and Cookson (1955) documented *Cyclonephelium compactum* and *C. distinctum* from the Australian Cenomanian deposits. The first downhole occurrence of *Coronifera oceanica* has been reported in the upper Cenomanian deposits of Paris Basin in France (Fauconnier, 1979) and from the Portuguese Western Basin in Portugal (Hasenboehler, 1981). In South Africa, Davey (1969) recorded *Exochosphaeridium bifidum* from a Cenomanian succession in northern Natal.

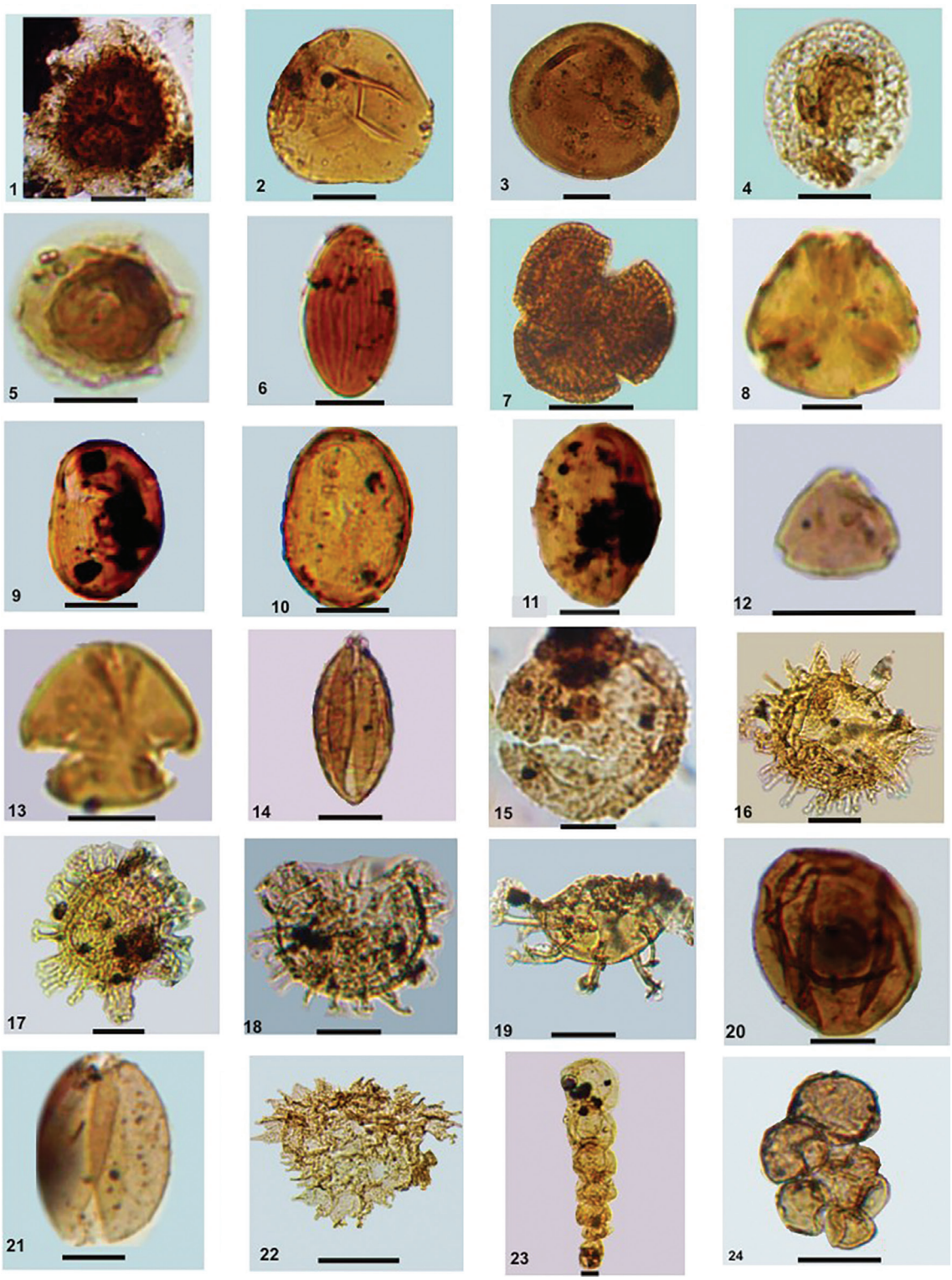

Figure 5: Transmitted light photomicrographs of various palynomorphs of the Raha Formation (Cenomanian), well name, sample depth, and the slide number; all scale bars are 20 µm. (1) *Crybelosporites pannuceus* (Brenner, 1963) Srivastava, 1977; B-115, 1,011 m, slide B. (2) *Cyathidites australis* Couper, 1953; B-109, 891 m, Slide B. (3) *Araucariacites australis* Cookson, 1947 ex Couper, 1953; B-109, 879 m, Slide C. (4) *Afropollis jardinus* (Brenner) Doyle et al. 1982; B-114, 1,008 m, Slide C. (5) *Callialasporites discoidalis* (Doring) Bharad and Kumar 1972; B-109, 891 m, Slide B. (6) *Ephedripites* sp.; B-109, 903 m, Slide A. (7) *Rousea delicipollis* Srivastava, 1977; B-109, 894 m, Slide C. (8) *Nyssapollenites* sp.; B-115, 1,023 m, Slide B. (9) *Classopollis brasiliensis* Herngreen, 1975; B-114, 987 m, Slide A. (10) *Classopollis* cf. *brasiliensis* Herngreen, 1975; B-114, 987 m, Slide A. (11) *Classopollis* cf. *brasiliensis* Herngreen, 1975; B-114, 987 m, Slide A. (12) *Triporites* sp.; B-109, 894 m, Slide A. (13) *T. sagax* Couper, 1960; B-109, 897 m, Slide B. (14) *T. sagax* Couper, 1960; (equatorial view) B-109, 891 m, Slide A. (15) *Trichodinium castanea* Deflandre, 1935 ex Clarke and Verdier, 1967; B-114, 966 m, Slide A. (16) *Systematophora* aff. *cretacea* Davey, 1979; B-115, 1,023 m, Slide C. (17) *Coronifera oceanica* Cookson and Eisenack, 1958; B-115, 990 m, Slide A. (18) *Circulodinium distinctum* (Deflandre and Cookson, 1955) Jansonius, 1986; B-115, 1,023 m, Slide A. (19) *Hystrichosphaeridium recurvatum* (White, 1842) Lejeune-Carpentier, 1940; B-115, 996 m, slide A. (20) *Leiosphaeridium* sp.; B-115, 993 m, Slide B. (21) Ovoidites parvus (Cookson and Dettmann) Nakoman, 1966; B-109, 888 m, slide B. (22) Pediastrum boryanum (Turpin 1828) Meneghini 1,840; B-115, 1,023 m, slide B. (23) Microforaminiferal test lining; B-109, 891 m, slide A. (24) Microforaminiferal test lining; B-109, 891 m, Slide A.

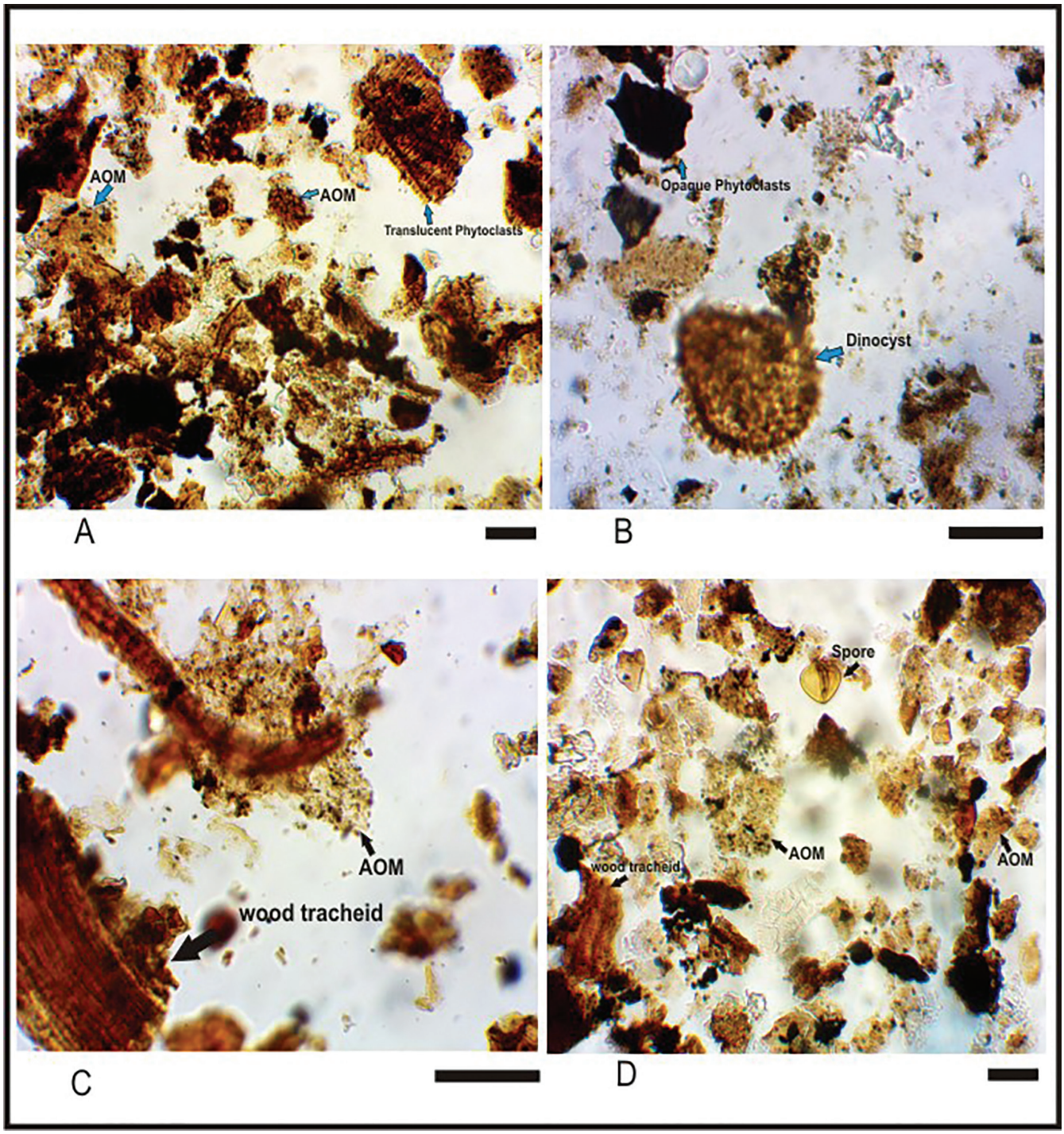

Figure 6: Transmitted light photomicrograph of palynofacies components encountered within the rock samples of the Raha Formation. A, C represent palynofacies associations of B-114; B shows a palynofacies assemblage of B-115; and D represents a palynofacies assemblage of B-109.

5.1.2. Palynozone II *Afropollis jardinus–Crybelosporites pannuceus* Assemblage Zone

Zone definition

This zone is defined by the first downhole occurrence of *Afropollis jardinus* and *Crybelosporites pannuceus*, extended downwards to the base of studied wells.

Occurrence

In B-114, this zone occurred at a depth ranging from 1,038 m to 987 m (51 m thick) of the Raha Formation, while in B-109, it occurred from 975 m to 915 m depth (60 m thick); in B-115, it occurred from 1,023 m to 987 m depth (36 m thick) of the Raha Formation (Figs. 4 and 5).

Diagnosis

Beside the marker species of this zone, other important taxa such as the angiosperm *Retimonocolpites variplicatus* and the marine dinocysts *Florentinia deanei, Florentinia* spp., *Circulodinium distinctum* and *C. compactum* are recorded.

Associated taxa

Exesipollenites spp., *Monocolpopollenites* spp., *Classopollis torosus*, *Balmeiopsis limbatus*, *Araucariacites australis*,

Zonation										Age
This Study	Tahoun and Deaf (2016)	Tahoun and Mohamed (2013)	Thusu et al (1988)	Batten and Uwins (1985)	Schrank and Awad (1990)	Lawal and Moullade (1986)	Olde et al., (2014)	Čech et al., (2005)	Davey et al. (1966)	
Gulf of Suez Egypt	Western Desert Egypt		Libya		Sudan	Nigeria	Bohemian Basin Czech Republic		Fetcham Mill England	
Classopollis brasiliensis *Tricolpites sagax*	*Classopollis brasiliensis* *Dinopterygium cladoidesis*		*Classopollis brasiliensis*		*Tricolpites sagax*	*Classopollis brasiliensis* *Triorites africaensis*	*Litosphaeridium siphoniphorum*	The triporate angiosperm pollen *Complexiopollis* spp.	*Hystrichosphaeridium readei* *Hystrichosphaeridium radiculatum*	late Cenomanian
Crybelosporites pannuceus *Afropollis jardinus*	*Crybelosporites pannuceus* *Afropollis jardinus*	*Trilobosporites laevigatus* *Cretacaeiporites densimurus* *Elaterosporites klaszii* *Afropollis jardinus*		*Crybelosporites pannuceus* *Afropollis jardinus*		*Afropollis jardinus*			*Oligosphaeridium prolixispinosum*	early-middle Cenomanian

Figure 7: Various palynomorph zonations of the Cenomanian strata from the Egyptian territory and globally from the neighbouring countries and northern Europe. Major absence of specific intervals are coloured grey in the zonation chart.

A. hungaricus, Inaperturopollenites spp., *Spheripollenites* spp., *Foveotricolpites* spp., *Arecipites* spp. and *Exochosphaeridium bifidum* are documented within this interval (Figs. 4 and 5).

Proposed age

The presumed age is early-middle Cenomanian.

Correlation

Afropollis jardinus, a characteristic species has been recorded for the first time in the lower-middle Cenomanian deposits of northern Gondwana (Doyle et al., 1982). The stratigraphically important *Afropollis jardinus* and *Crybelosporites pannuceus* characterise the Cenomanian sediments, and their first downhole appearances were repeatedly reported from the following regions: the lower-middle Cenomanian strata of Egypt in the Qattara Depression, northern part of the Western Desert (Ibrahim, 1996); an outcrop succession of the Dakhla Oasis in the central region of the Western Desert (Schrank and Mahmoud, 1998); and the subsurface succession of the Bahariya Formation, northern region of the Western Desert (Tahoun and Mohamed, 2013). The top range of the sporomorphs *A. jardinus* and *C. pannuceus* were documented from the lower-middle Cenomanian subsurface intervals of the northern region of the Western Desert of Egypt (e.g. Sultan and Aly, 1986; Aboul Ela and Mahrous, 1992; Schrank and Ibrahim, 1995; El Beialy et al. 2010, 2011). Furthermore, Ibrahim (2002) documented the last appearance datum of these two taxa as the middle-late Cenomanian boundary.

Globally, Hasenboehler (1981) documented such marker taxa from the early-middle Cenomanian of the Portuguese Western Basin of Portugal. Moreover, Schrank (1990) identified the same species in the lower-middle Cenomanian strata of the clastic sediments between Dongola and Wadi Muqaddam in northern Sudan. (In northeast Libya, Batten and Uwins (1985) recorded the common occurrence of *Afropollis* cf. *jardinus* and *Crybelosporites* sp. from subsurface succession of the northern part of the Cyrenaica Shelf. In Northeastern Nigeria, Lawal and Moullade (1986) documented *A. jardinus* and *Hexaporotricolpites potoniei* with an age no younger than early-middle Cenomanian in the lower part of Zone I (Subzone Ia) in the Upper Benue Basin. However, the latter species are not recorded within the sedimentary succession all over Egypt.

On the contrary, Mahmoud et al. (2007) recorded the topmost appearances of *Retimonocolpites variplicatus* within the early Cenomanian from the onshore sediments of the northern part of the Gulf of Suez, Egypt. Recently, Tahoun and Mohamed (2013) recorded the same bioevent for *R. variplicatus* in the early Cenomanian of the northern region of Western Desert of Egypt.

Florentinia deanei and other *Florentinia* spp. were abundantly reported from the lower-middle Cenomanian in Egypt and the Tethyan Realm. In the Gulf of Suez area, Mahmoud et al. (2007) recorded *Florentinia laciniata* and *F. resex* in the lower Cenomanian succession. *Cyclonephelium compactum* and *C. distinctum* were recorded from the Australian lower Cenomanian deposits (Deflandre and Cookson, 1955). Similar specimens were previously recorded from the Cenomanian in the Tethys region. *F. laciniata* has been recorded in France by Courtinat et al. (1991) and in Portugal by Hasenboehler (1981). Moreover, *Florentinia deanei* has been recorded by Davey (1969) and Foucher (1979) in France.

However, poor recovery of the lower-middle Cenomanian strata of the Raha Formation, followed mainly by the exhaustive disappearance of palynological assemblages in several samples, may be related to unfavourable lithologies (Peyrot et al., 2011). Pearce et al. (2009) also pointed out to low palynomorph recovery, especially dinocysts, in improper sediments, which are responsible for such vulnerable-to-absent palynomorph preservation.

5.2. Palynofacies distribution

Palynofacies is a term commonly used to describe the total particulate organic matter (POM) assemblage contained in a body of sediment thought to reflect a specific set of environmental conditions or to be associated with a characteristic range of hydrocarbon-generating potential (Tyson, 1995). The main targets of palynofacies investigation are demonstration of the proximal–distal trends of the shoreline along with major transgressive–regressive episodes of the sea level, as well as to interpret the environmental conditions of the Raha Formation, thus, contributing to the knowledge on the geological evolution during the Cenomanian of the Gulf of Suez in general, and the Bakr Field in particular.

In B-114, the first assemblage of the investigated samples extends from 1,035 m to 1,008 m, with samples at separate depths of 993, 990, 981, 966, 957, 954 and 948 m. This association is characterised by a relatively high abundance of phytoclasts (59.4%–41.1%) and AOM (58.9%–38.5%), with a low percentage of palynomorphs (5.2%–0%). However, the second group of samples spans depths of 1,038, 969, 963, 960 and 951 m, which are characterised by a dominant high abundance of phytoclasts (79.9% at a depth of 969 m, to 64.5% at a depth of 963 m), moderate-to-low abundance of AOM (35.5%–18.5%) and very low abundance of palynomorphs (0%–1.7%) (Table 4 in Supplementary data). The third group, hosting the samples at depths of 945, 972, 975, 987, 996 and 1,005 m, is characterised by an overabundance of AOM (90.7%–64.4%), moderate-to-low phytoclasts (36.8%–8.6%) and low abundance of palynomorphs (7.9%–0%) (Table 4 in Supplementary data). Consequently, the translucent phytoclasts are basically greater than the opaque woody particles throughout the borehole. However, in the third group, the opaque phytoclasts, which dominate over the translucent particles (7.7%–1.8%), range from 21.4% to 6.6%. In addition, the equidimensional opaque phytoclasts represent an overwhelming majority rather than the lath-shaped opaque debris throughout the succession (Fig. 7).

In B-115, samples at depths of 996, 999, 1,005, 1,008, 1,011 and 1,023 m have high abundance of AOM

(57.8%–42.3%), with high–to-moderate abundance of phytoclasts (56.5%–31.9%) and moderate–to-low abundance of palynomorphs (19.6% at a depth of 1,011 m to 0.6% at a depth of 999 m). Generally, the phytoclasts herein are overwhelmingly dominated by the opaque particles and particularly reach their maxima at depths of 999 m and 1,008 m. The sporomorph count reaches its maximum peak compared to the low dinocyst count at a depth of 1,011 m. Furthermore, the foraminiferal test linings record a remarkable percentage up to 2.9% at a depth of 1,023 m (Table 5 in Supplementary data). The samples, which include depths of 987–993, 1,002 and 1,014–1,020 m, are dominated by a plethora of AOM (89.8%–66.4%), with moderate-to-low abundance of phytoclasts (32.1%–5.1%) and low-to-no occurrence of palynomorphs (5.2%–0%) (Table 5 in Supplementary data). It is worth mentioning that samples at depths of 1,017 m and 1,020 m seem to be distinctive within a local red-shale horizon. However, in this interval, the richness of palynomorphs decreases markedly, from five specimens of both pollen grains and dinoflagellate cysts at 1,020 m depth to absent at 1,017 m. Consequently, the preserved individuals reveal reddish brown colour as a consequence of oxidation, whereas a typical distortion of two undefined specimens of pollen grains and dinoflagellates is attributed to abnormal concentration of iron oxides (Fig. 8).

In B-109, samples at depths of 915, 906–903, 897, 891 and 876–885 m are characterised by AOM richness (89%–60.5%), with relatively moderate abundance of phytoclasts (25.1%–10.1%) and moderate-to-low content of palynomorphs (15.2%–2.5%) (Table 6 in Supplementary data). However, the total sporomorph count records three peaks at depths of 906, 903 and 897 m, with approximate counts of 125–150 individuals, whereas the total dinocyst count records two peaks at depths of 897 and 879 m, respectively. The second group of B-109, located at depths of 975-918, 909, 900, 894, and 888 m, is predominantly characterised by high abundance of phytoclasts (69.9%–28%), high abundance of AOM (58.4%–30.1%), with low-to-negligible abundance of palynomorphs (15.3%–0%) (Table 6 in Supplementary data). Moreover, the translucent phytoclasts have convergent abundance with the opaque debris throughout the borehole. The sporomorph count records two main peaks at depths of 900 m and 888 m, together with a noticeable peak of the marine/terrestrial ratio recorded at a depth of 894 m (Fig. 9).

In summary, there is a successive fluctuation of the POM constituent throughout the three wells. However, the lateral observation of organic particles between the three sections indicates predominantly similar kerogen abundances and composition. The recorded palynomorphs are mostly terrestrial representatives such as spores and pollen grains, whereas marine representative palynomorphs of dinocysts and microforaminiferal test linings are also recorded, yet in very low abundances.

5.3. Palynofacies and palaeoenvironmental implication

For a detailed palaeoenvironmental study based on palynofacies, a quantification of the kerogen content and composition was carried out. Both the composition of POM and its distribution are controlled by the influence of ecological and sedimentological processes within the physical environment. The compositional change of POM indicates significant information for palaeoenvironmental interpretation in terms of transgressive–regressive trends and relative sea-level changes (Harker et al., 1990; Tyson, 1995; Batten, 1996; Pittet and Gorin, 1997; Tahoun and Deaf, 2016; Mansour et al., 2018). The POM group is the product of compiling various factors (i.e. marine palynomorph versus terrestrial influx, source and rate of sediment influx, water salinity, depth, oxygen concentrations, and so on) within a given depositional environment (Tyson, 1993; Pittet and Gorin, 1997; Tahoun, 2012; Tahoun et al., 2013, 2017).

Herein, electrical well log data (e.g. logs of gamma ray, density and neutron porosity) could principally assist in interpreting the depositional palaeoenvironments. Changes in the gamma ray data reflect the lithological facies and their vertical variations based upon their grain sizes throughout the successions. Thereby, fine-grained sand facies usually are shale rich and, consequently, have higher gamma-ray values and vice versa, whereas carbonate facies commonly have lower gamma-ray readings (Rider, 2004).

In this study, all samples of the Raha Formation are plotted in the AOM-Phytoclast-Palynomorph ternary diagram after Tyson (1993, 1995) (Fig. 3). This plot is used to indicate various types of kerogen assemblages, the redox status of the depositional environments, proximity to terrestrial organic matter sources, as well as relative proximity to kerogen transport paths. However, the proximal–distal trend considers one of the main factors controlling the kerogen distribution. On the other hand, the documented palynomorphs, either terrestrially derived or marine-inhabited palynomorphs, are utilised to illustrate dissimilarities during deposition of the Raha Formation (Figs. 8–10). Both spores and pollen grains in the studied samples are considered as major constituents of the total palynomorphs content compared to dinocysts and acritarchs. These terrestrial palynomorphs are mainly used as substantial indicators of the conspicuous allochthonous fluviatile input as well as proximity to shoreline trends within the depositional palaeoenvironment (Tyson, 1995; Pittet and Gorin, 1997; Tahoun et al., 2017; Mansour et al., 2018).

The Cenomanian Raha Formation and its equivalents all over Egypt have been deposited in a shallow marine environment during the major Cenomanian transgression (Kerdany and Cherif, 1990; Schütz, 1994; Anan et al., 2013; El Fawal et al., 2014). The qualitative and quantitative analyses of POM constituents encountered within the Raha Formation indicate three depositional palaeoenvironmental settings.

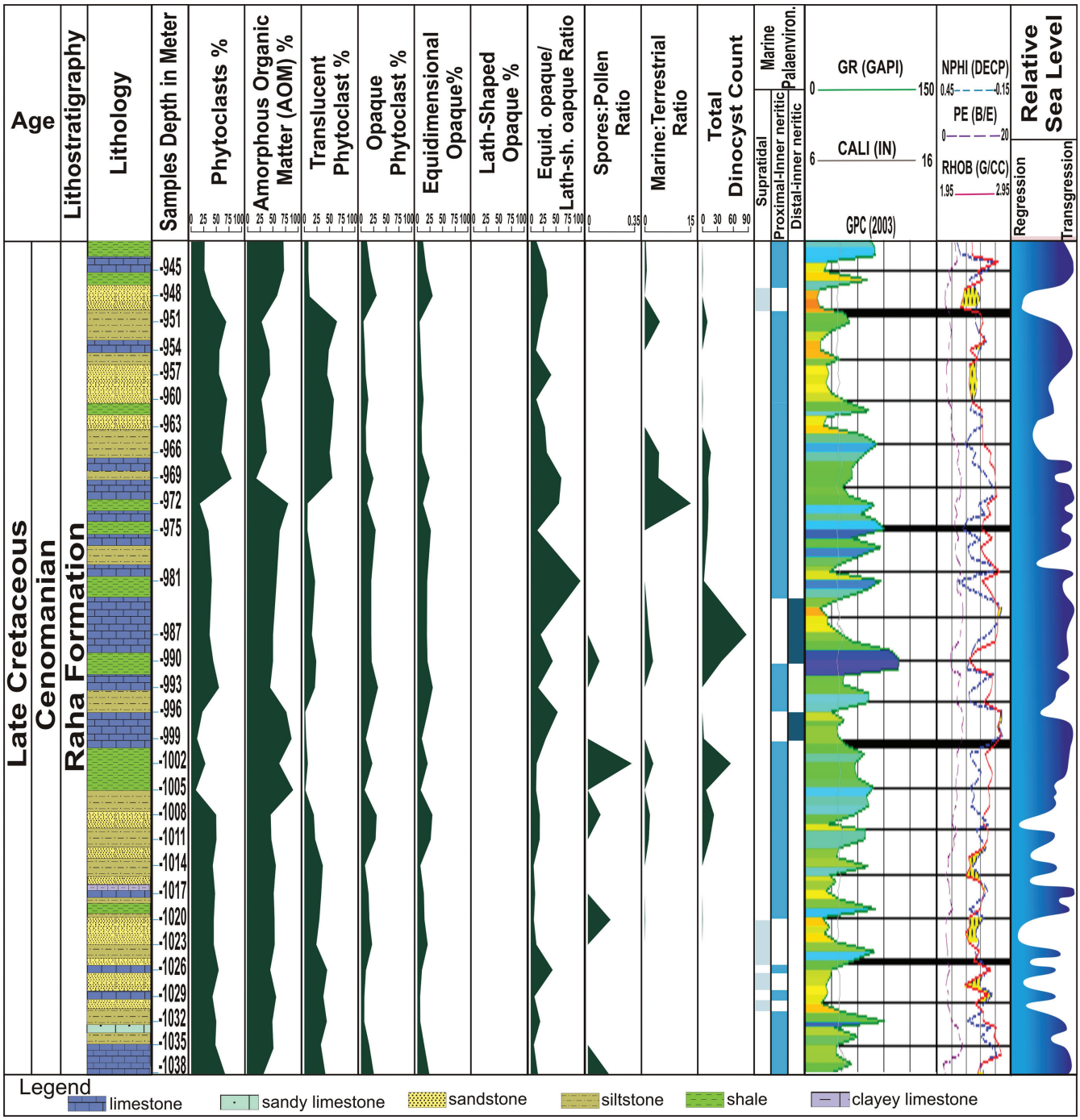

Figure 8: Sedimentary organic material distribution and palaeoenvironmental indication of B-114 well.

5.3.1. Supratidal environment

The supratidal environment developed in areas above normal high tide, where storms are the only flooding dynamic process (Schlager, 2005). It is characterised by the deposition of coastal dunes developed by aeolian transport and reworked sand from adjacent beaches (Perry and Taylor, 2007). In addition, the window of marine carbonate production decreases to zero in such conditions (Schlager, 2005). The supratidal environment has been repeatedly reported at different intervals of the Raha Formation. In B-114, it alternates with inner neritic environment from 1,031 m to 1,020 m, whereas in B-109, it covers an interval from 972 m to 966 m (Figs. 8 and 10).

The deposits of the supratidal environment are characterised by convergent percentages of the AOM and phytoclasts. The onshore to shallow supratidal setting is supported by the dominance of translucent and equidimensional opaque phytoclasts. However, the dominance of the translucent phytoclasts over opaque particles indicates a strong terrestrial influx and, therefore, suggests deposition in a nearshore proximal setting (Tyson, 1989). In contrast, equidimensional opaque particles are the foremost constituent compared with the lath-shaped

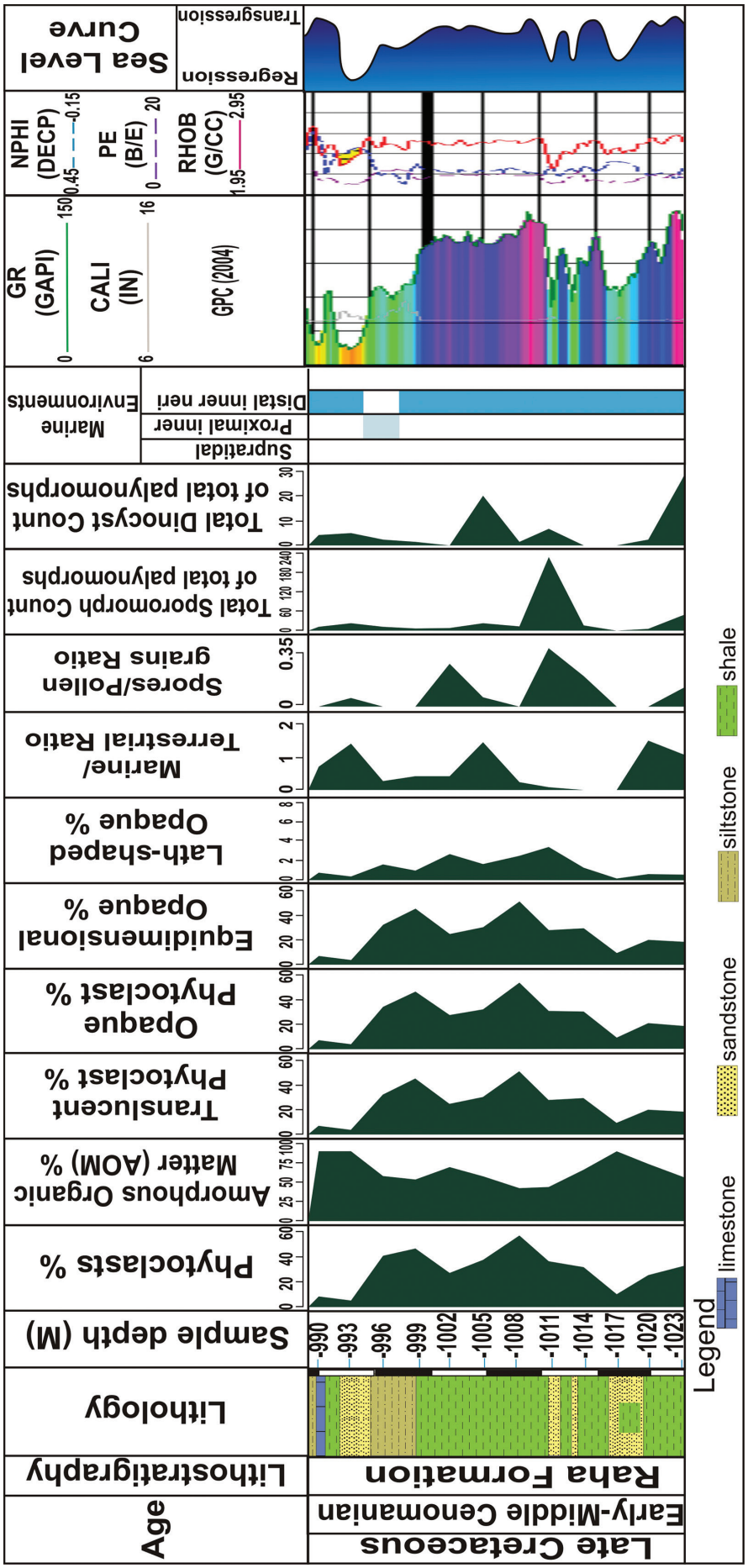

Figure 9: Sedimentary organic material distribution and palaeoenvironmental indication of B-115 well.

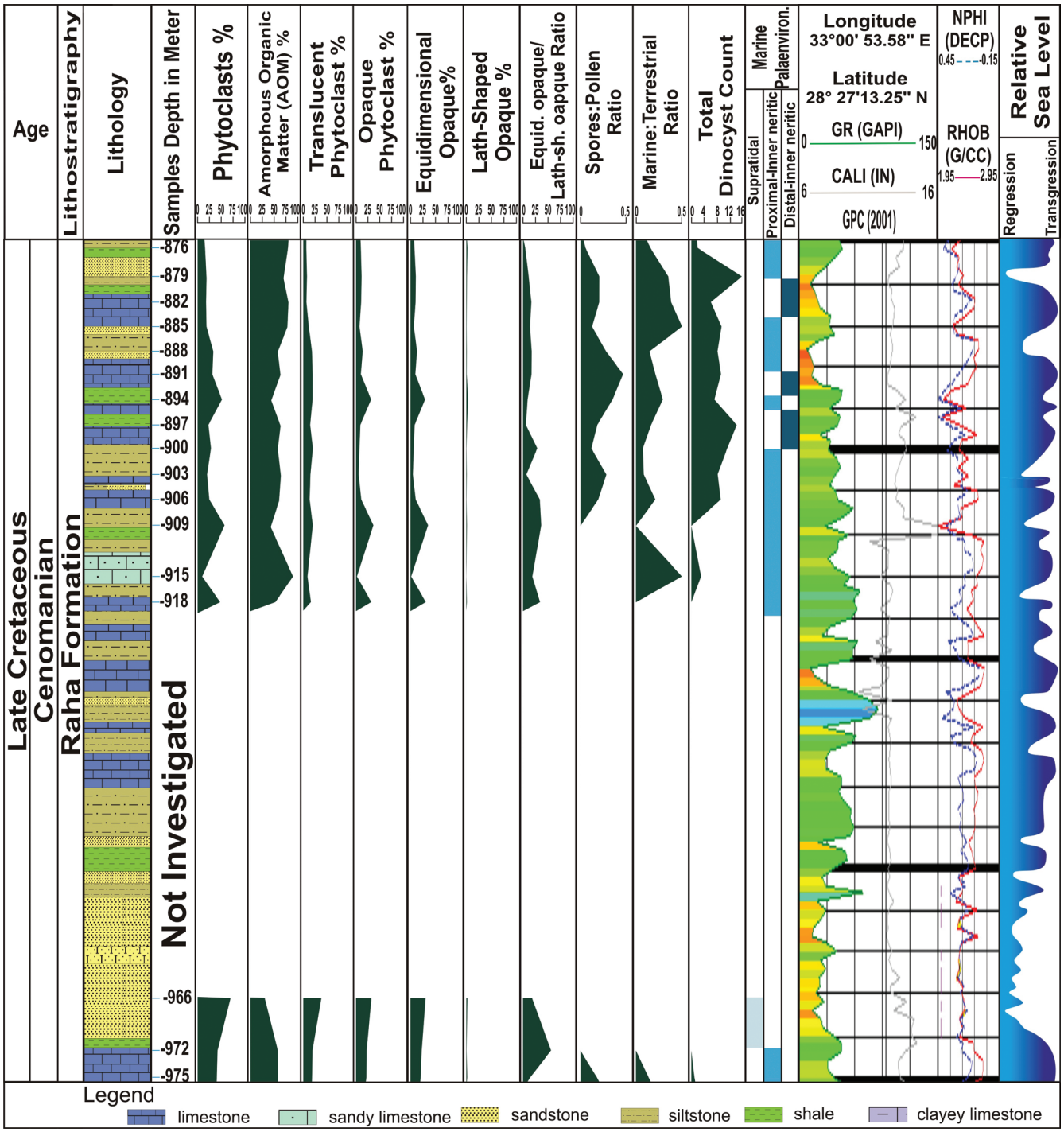

Figure 10: Sedimentary organic material distribution and palaeoenvironmental indication of B-109 well.

opaque particles, which in turn is controlled by the hydrodynamic equivalence and, thus, indicates a pronounced shore proximity during deposition (Tyson, 1995; Pittet and Gorin, 1997; Tahoun et al., 2013; Tahoun et al., 2017). The marine/terrestrial ratio records a very low to negligible percentage, indicating deposition above normal high tide. Moreover, the relative absence of marine palynomorphs (e.g. dinoflagellate cysts) and the very poor sporomorph count reflect deposition in a proximal onshore environment (Tyson, 1993, 1995; Pittet and Gorin, 1997; Mansour et al., 2018). Generally, the supratidal deposits have a very poor to absent palynomorph record. The previous palynological criteria strongly underpinned the deposition of these intervals in a shallowing supratidal environment (Figs. 8–10).

5.3.2. Proximal inner neritic environment

The shallow neritic or subtidal environment was defined by Ahr (2008) as the submerged zone that extends from the lowest low tide line to a relative depth of 200 m, without depth designation that distinguishes among inner, middle and outer neritic environments.

Based upon the integration of the palynologic and the lithologic data, proximal inner neritic conditions are considered the main environment during deposition of the Raha Formation. However, the palynofacies association in most samples of the proximal inner neritic deposits is dominated by AOM and phytoclasts. This is particularly related to various controlling factors (e.g. the minor fluctuation of the relative sea level along with the proximity to the coastline, as well as terrestrial/fresh water influx). The equidimensional opaque particles exhibit higher percentages than the lath-shaped opaque debris. These parameters markedly reflect the same above-mentioned scenario based on hydrodynamic equivalence of the micro-fragment woody particles and strongly suggest deposition in shallower proximal inner neritic environment (Tyson, 1995; Pittet and Gorin, 1997; Tahoun et al., 2013; Tahoun and Deaf, 2016; Tahoun et al., 2017; Mansour et al., 2018).

The quantitative distribution is commonly dominated by pollen grains in all samples that are deposited within proximal inner neritic shelf environment. The herein-reported *Araucariacites*, which mainly inhabits areas of dry hinterland (Schrank and Mahmoud, 1998), is, by far, the main constituent of gymnosperms. *Araucariacites*, *Classopollis* and *Spheripollenites* altogether made up >70% of the total counted pollen grains (Supplementary data: Tables 1 and 3). The relative abundance of *Afropollis* and *Ephedripites* pollen indicates an arid to semi-arid warm climatic conditions (e.g. Mahmoud and Moawad, 2002). These pollen-producing plants commonly inhabit in palaeotropical humid coastal plains (Schrank, 2001; El Beialy et al., 2011). However, their prevalence with marine phytoplankton in the Raha Formation appears to be partially driven by hydrodynamic properties during pronounced terrigenous sediment influx and deposition in shallow water environment.

The spores are usually documented in considerable counts at depths of 879, 888, 903 and 906 m in B-109, at a depth of 1,011 m in B-115 (up to 58 individuals) and at 1,002 m in B-114 m (Supplementary data: Tables 4–6) (Figs. 9 and 10). The pteridophytic spore associations in such samples are dominated by *Cyathidites, Deltoidospora, Crybelosporites* and *Biretisporites*. The presence of the fern groups *Cyathidites* and *Deltoidospora*, growing on wet biotopes under warm subtropical conditions (Kedves, 1986; Schrank and Mahmoud, 1998), indicates that such intervals have been deposited close to active terrigenous sediment influx. The water fern spore *Crybelosporites* inhabits mainly freshwater bodies (e.g. ponds and/or lakes, Mahmoud and Moawad, 2002), thus also reinforcing the conspicuous terrestrial influx and deposition in proximal shallow-marine environments.

In contrast, samples at depths of 1,008, 1,002 and 990 m in B-114 have AOM proliferation and marine palynomorph (e.g. dinoflagellate cysts) content (Fig. 8), which may represent a transgressive phase. Further, in B-115, two noticeable peaks of the total dinocyst count are reported at depths of 1,005 m and 1,023 m, whereas in B-109, three remarkable peaks are recorded at depths of 879, 885 and 906 m. The relative abundance of the documented dinocysts in the aforementioned samples is dominated by the gonyaulacoid cysts *Cyclonephelium*, *Heterosphaeridium*, *Florentinia, Systematophora* and *Exochosphaeridium,* with rare occurrence of *Spiniferites*. The gonyaulacoid dinocyst genus *Cyclonephelium* is mainly attributed to warm, marginal marine, proximal inner neritic conditions (Brinkhuis and Zachariasse, 1988; Eshet et al., 1992; Brinkhuis, 1994). However, the presence of *Spiniferites, Exochosphaeridium* and *Florentinia* is commonly related to open marine, outer shelf settings, which are impoverished and sparsely recorded in these intervals (Marshall and Batten, 1988; Brinkhuis, 1994).

On the other hand, it is worth mentioning that samples at depths of 1,020 m and 1,017 m in B-115 are dominated by iron-rich shale. Nonetheless, the petrographic analysis of these samples under a microscope clearly shows a flaky, silty fissile structure. Therefore, this Fe-rich shale facies indicates that the primary sedimentary structure of shale is well preserved. So, we suggest that it was formed syndepositionally in an oxygen-rich environment (Tucker, 2001). In contrast, Mansour et al. (2018) located a sequence boundary within this interval and illustrated that it was deposited primarily during a stage of relative fall of sea level in a shallow proximal inner neritic zone, where the conditions were highly oxic. The palynofacies assemblages indicate proximal oxic–suboxic to –anoxic shelf conditions as deduced from the ternary plot of Tyson (1995) (Fig. 3).

5.3.3. Distal inner neritic environment

The distal inner neritic environment has been recorded at different intervals of the Raha Formation. In B-114, it occurs at depths of 999–996 m and 990–983 m (Fig. 8), whereas in B-109, it occurs at depths of 900–879 m (Fig. 10), which was accompanied by a consecutive minor fluctuation within a proximal inner neritic environment, which resulted from successive changes of the relative sea level.

The distal inner neritic deposits are mainly dominated by shales and limestones. The gamma ray values of the distal inner neritic facies are generally high in case of shale and very low to negligible in case of limestone and carbonate. Therefore, a drastic rise of the relative sea level is suggested owing to a drastic decrease of grain sizes, where the sedimentary facies tend to be shale rich, and a deepening trend during deposition can be deduced (Mansour et al., 2018). All samples of the distal inner neritic deposits are overwhelmingly dominated by AOM in B-114 (for instance, up to 87.3% at a depth of 999 m) as opposed to their equivalents in B-109. Consequently, the AOM characterises stagnant, low-energy, oxygen-depleted environments (Tyson, 1987). It gives an indication of shallower conditions and proximity of shoreline towards the south, where B-109 is located (Figs. 8 and 10). Moderate-to-high marine/terrestrial ratio occurs throughout the distal inner neritic intervals, with significant

peaks recorded at depths of 894, 882 and 879 m in B-109. However, wind-transported pollen grains are the major constituent of the total sporomorph count as opposed to negligible pteridophyte spores, which reinforced by low spores/pollen ratio, indicates a relatively distal marine setting (Lister and Batten, 1988; Tyson, 1993; Tahoun et al., 2017; Mansour et al., 2018). It is basically dominated by the gymnosperm *Classopollis,* reflecting derivation from coniferous plants, xerophyte precursors likely related to lagoonal and/or back-barrier islands (Peyrot et al., 2011) and probably deposited during major transgression of the sea level in areas at far distance from the site of its origin (Yi et al., 2003). In addition, the distribution of the *Araucariacites* group is usually common but less contrasted than the intervals of the above-mentioned environment (Supplementary data: Tables 1 and 3), reflecting relatively deeper conditions during deposition.

By contrast, remarkable peaks of the dinocyst count are documented at a depth of 987 m in B-114 and at depths of 900, 897 and 879 m in B-109 (Figs. 8 and 10). In B-114, the dinocyst assemblage is dominated by *Heterosphaeridium*, *Trichodinium, Florentinia, Spiniferites* and *Oligosphaeridium*, whereas in B-109, the skolochorate dinocyst *Florentinia, Spiniferites* and *Oligosphaeridium* groups are absent. In this context, the dinocyst-dominated assemblages corresponded to deeper conditions of sea level towards the north where B-114 is located, and a distal inner neritic environment is suggested. Furthermore, *Trichodinium castanea,* like the *Spiniferites* group, exhibits a deeper setting (Peyrot et al., 2011). Freshwater algae and achritarchs are sparsely recorded through the Raha Formation and point to a relative marine transgression.

Lower counts of spores to zero are significantly paralleled by the combined predominance of the spheroidal pollen grains and dinocysts strongly linked to a pronounced marine incursion of relative sea level (Lister and Batten, 1988; Tyson, 1993; Tahoun et al., 2017). The palynofacies assemblages of the herein-documented intervals indicate distal suboxic–anoxic shelf conditions as inferred from the ternary diagram of Tyson (1995), which plot in the palynofacies field IX (Fig. 3). The previous palynofacies and palynological clues that confirm distal positions from a terrestrial input and increasing autochthonous marine constituents, therefore, strengthen our result as a distal inner neritic environment.

5.4. Palaeobiogeographic implication

The sporomorphs could be effectively used in delineating the floral provinces and as supporting good evidences for palaeobiogeography. Since the Cretaceous time, immense phytogeographic differences in the vegetation all over the world have been documented (Brenner, 1976). During the mid-Cretaceous time, four latitudinally controlled floristic provinces that are characterised by distinct palynofloristic features can be distinguished (Batten, 1984).

In the present study, the recovered sporomorphs show remarkable diversity and abundance of various gymnosperms, such as *Araucariacites*, *Classopollis*, *Cycadopites* and *Ephedripites,* and a relatively homogeneous diversity pattern of angiosperm pollen such as *Afropollis*, *Tricolpites* and *Retimonocolpites*. Moreover, the low diversity of pteridophyte spores, represented mainly by *Deltoidospora,* is coupled with the rare occurrence of bisaccate pollen versus the common occurrence of the marker *Crybelosporites*. Such sporomorphs show collectively striking similarity to the low-latitude, equatorial, Northern Gondwana province (Hochuli, 1981), African–South American (ASA) province (Herngreen and Chlonova, 1981) or its recent alternative elaterate Albian–Cenomanian microfloral province (Herngreen et al., 1996) (Fig. 11).

The only notable difference from the typical assemblage of the ASA province is the absence of elater-bearing forms in the present material. Such elater-bearing pollen typifies the late Albian–Cenomanian times and is enhanced in number and specific diversity during the Cenomanian. Doyle et al. (1982) accounted for these endemic taxa to be concentrated and appear amply in the mid-Cretaceous of equatorial regions (Brazil, Gabon, Ghana and Senegal). It is worth remarking that the diversity of these flora declines to the northward and northwestward direction from the equator. Their quantity decreases towards the north of Egypt, Sinai, Libya, Tunisia, and Morocco and also to the south of Patagonia and Madagascar, where bisaccate and trisaccate pollen are dominating. According to Herngreen and Chlonova (1981), the species diversity of the elater-bearing sporomorphs is thriving in the axial zone of the mid-Cretaceous ASA microfloral province, which is close to the palaeoequator as reconstructed by Phillips and Forsyth (1972). Moreover, Herngreen and Chlonova (1981) assumed that the southern boundary of the ASA province may preliminarily be drawn through the northernmost part of South America, Surinam offshore from Peru, Northeastern Brazil via West Africa, while the northern boundary may be drawn through the northern part of South America, extending to Senegal and via Algeria, Tunisia and Egypt to Israel.

The absence of elaters from the present material exhibits minor differences in the type of flora than those recorded from the equatorial regions. This may be attributed to some climatic difference from the hot tropical climate at the equator to a humid subtropical climate towards the north. Moreover, it may strongly imply proximity to the separating northern discontinuity boundary of the Northern Gondwana Province, with a transitional affiliation for Egypt between the Northern Gondwana Province and the Southern Laurasia Province (Brenner, 1976). However, the temporal and geographical distribution of such assemblages may substantially be facies dependent, or elevation to full zonal status is reserved until further ongoing research in the Gulf region is complete (Paterson and Mangerud, 2015). But the common occurrence of elaters documented in the middle Albian–Cenomanian of the northern part of the Western Desert (Schrank, 2000; El Beialy et al., 2010; Tahoun et al., 2012;

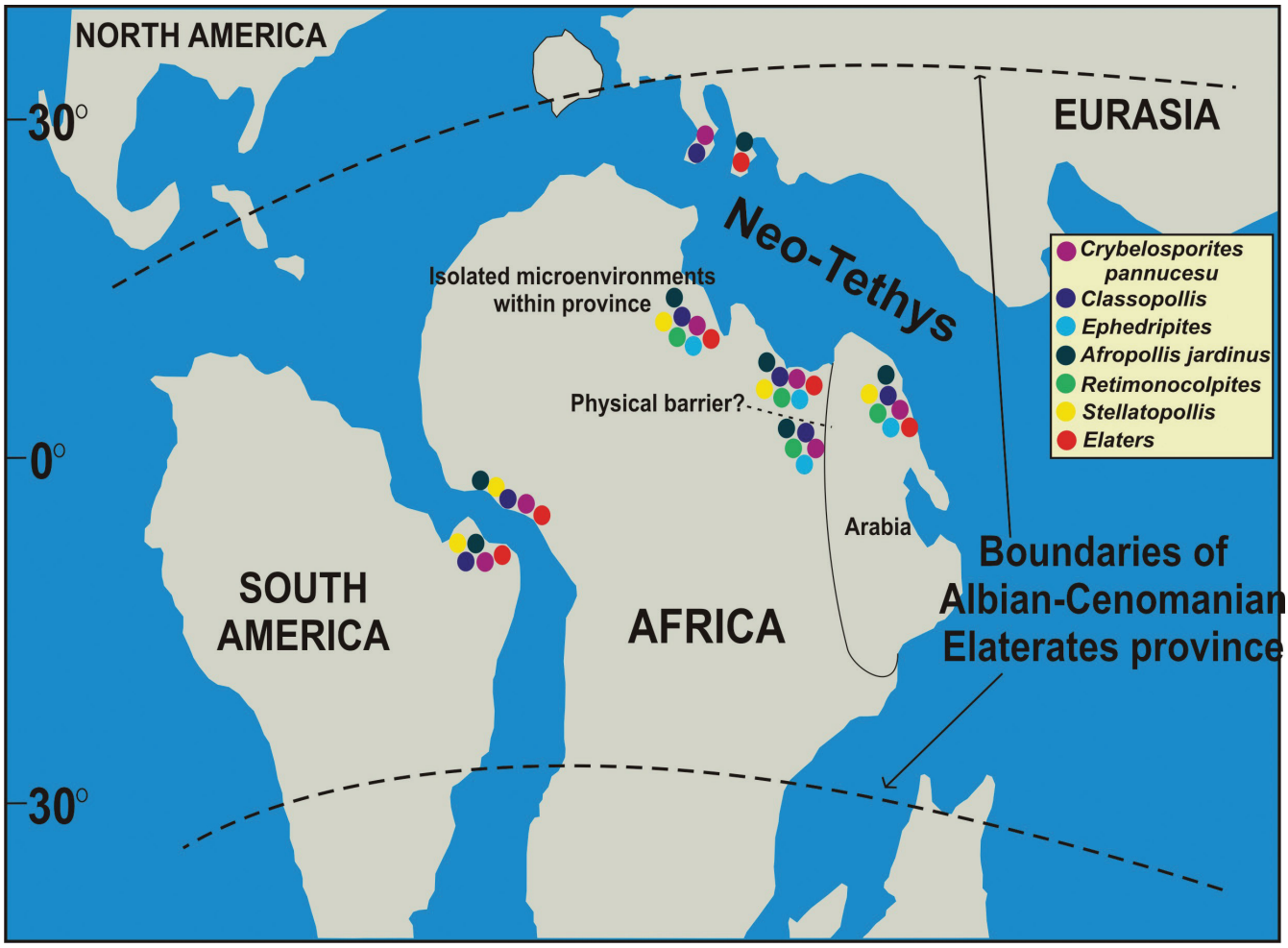

Figure 11: The proposed presence of environment-controlled small niche or micro-environments in the studied area within the boundaries of Albian–Cenomanian elaterate province based on the complete absence of elater-bearing pollen in the present material (modified after Herngreen et al. 1996; Ibrahim et al. 2000).

Tahoun and Mohamed, 2013; Tahoun et al., 2015), Libya (Thusu et al., 1988) and towards the north of the Gulf of Suez region (Deaf, 2009) negates this assumption. In addition, the proximity to the separating eastern boundary of the Northern Gondwana Province is not excluded, but the record in Qatar in the Arabian Gulf area (Ibrahim et al., 2000) contradicts this assumption, too (Fig. 11).

Batten and Li (1987) and Ibrahim et al. (2000) outlined that the geographic extent of the Albian–Cenomanian elaterate floral province is much greater than originally thought and that it has a far wider distribution, with new emphasis recorded from China and Papua New Guinea (Fig. 11). It is feasible at different scales to illustrate the remarkable compositional variations that include the absence of some taxa that relate directly to particular facies change within the defined environmental confines (Helby et al., 1987). The absence of elater-bearing forms may be explained as they have been come into eyesight extensively in the equatorial region, but to a lesser amplitude, they have been accounted for in Egypt. However, the complete absence of elaters may be attributed to the existence of a physical or biological barrier that hinders the distribution of such type of elaterate parent plants and results in considerable variances in sedimentological processes and remarkable limiting and controlling environmental conditions. Such a probable barrier may create various micro-environments or definite bio-niches in the site of deposition of the present study area.

6. Conclusions

The palynological analysis of the Cenomanian successions in the B-114, B-115 and B-109 wells of the BOF differentiates two palynozones: (1) the early-middle Cenomanian *Afropollis jardinus* and *Crybelosporites pannuceus* Assemblage zone (Palynozone II) assigned for the lower part of the Raha Formation; and (2) the late Cenomanian *C. brasiliensis* and *T. sagax* Assemblage zone (Palynozone I) allocated for the upper part of the Raha Formation. There are significant co-occurring palynomorph species, which provide a powerful tool for the biostratigraphic zonation, such as the dinocysts *Florentinia deanei, Florentinia* spp. within the lower-middle Cenomanian zone and the *Nyssapollenites* spp. and *Triporites* sp. in the upper Cenomanian succession.

In addition, a structural cross-section is constructed between the studied wells revealing the tectonic

overprinting of the Raha Formation, where a normal fault markedly eroded the upper part of the Raha Formation in B-115. The amalgamation between the palynological data, of specific spores, pollen grains and dinocysts commonly used as environmental indicators, and the palynofacies analysis has revealed that the depositional palaeoenvironment of the Raha Formation was deposited in a continental shelf setting fluctuating from supratidal to distal inner neritic conditions. Such conditions took place during the Neo-Tethyan transgression event, which inundated the African cratonic regions generally and the Gulf of Suez especially. Accordingly, this event was derived from the north where B-114 is located towards B-109 in the south.

The absence of elaters from the studied samples may be explained in terms of minor variation in the type of microflora, which may be attributed to some climatic dissimilarity and environment-controlled niche. In addition, it may be shaped by the existence of a physical barrier hindering the distribution of such type of elaterate parent plants.

Acknowledgements

We are grateful to the Egyptian General Petroleum Corporation (EGPC) for their permission to obtain the required data, as well as the authority of the General Petroleum Company (GPC) in Egypt for providing the e-logs and samples for the present study. Moreover, we would like to thank the journal editor Prof. Michael Wagreich and Assoc. Prof. Dr. Polina Pavlishina, Sofia University, Bulgaria, and another anonymous reviewer for their thorough revision and perceptive comments, which significantly improved the paper. This study was conducted as a part of the MSc dissertation research project of A. Mansour.

References

Abdallah, A.M., El-Adindani, A., 1963. Notes on the Cenomanian-Turonian contact in the Galala Plateau, Eastern Desert, Egypt. Egyptian Journal of Geology 7, 67–70.

Aboul Ela, N.M., Mahrous, H.A.R., 1992. Albian-Cenomanian miospores from the subsurface of the North Western Desert, Egypt. Neues Jahrbuch für Geologie und Paläontologie Monatshefte 10, 595–613.

Ahr, W.M., 2008. Geology of Carbonate Reservoirs; the identification, description, and characterization of hydrocarbon reservoirs in carbonate rocks, John Wiley & Sons, Canada, 277 pp.

Alsharhan, A.S., 2003. Petroleum geology and potential hydrocarbon plays in the Gulf of Suez rift basin, Egypt. American Association of Petroleum Geologists Bulletin 87, 143–180.

Anan, T.I., El-Shahat, A., Genedi, A., Grammer, M., 2013. Depositional environments and sequence architecture of the Raha and Abu Qada formations (Cenomanian-Turonian), west central Sinai, Egypt. Journal of African Earth Sciences 82, 54–69.

Awad, G.H., Abdallah, A.M., 1966. Upper Cretaceous in Southern Galala, Eastern Desert, with emphasis on neighboring areas. Journal of Geology of United Republic of Egypt 10, 125–142.

Azéma, C., Durand, S., Medus, J., 1972. Des miospores du Cenomanien Moyen. Paleobiologie continentale3, 1–54.

Batten, D.J., 1984. Palynology, climate and the development of Late Cretaceous floral provinces in the Northern Hemisphere, a review. In: P. J. Brenchley (ed), Fossils and Climate, (Edited by Brenchley, P.), Geological Journal, Special Issue 127–164. John Wiley, Chichester.

Batten, D.J., Li, W., 1987. Aspects of palynomorph distribution, floral provinces and climate during the Cretaceous. Geological Journal, Serial A 96, 219–237.

Batten, D.J., Uwins, P.J.R., 1985. Early-Late Cretaceous (Aptian-Cenomanian) palynomorphs. Journal of Micropaleontology, 4, 151–168.

Boltenhagen, E., 1980. Palynologie du Cretace superieur du Gabon. Memoires de la Section des Sciences, 7, 11–191.

Bosworth, W., McClay, K.R., 2001. Structural and stratigraphic evolution of the Gulf of Suez rift, Egypt: a synthesis. In: Zeigler, P.A., Cavazza, W., Robertson, A.H.F.R., Crasquin-Soleau, S. (Eds.), Peri-Tethys memoir 6: Peri-Tethyan rift/wrench basins and passive margins. Memoires du Museum National d'Histoire Naturelle de Paris 186, pp. 567–606.

Burden, E.T., Langille, A.B., 1991. Palynology of Cretaceous and Tertiary strata, northeast Baffin Island, Northwest Territories Canada; Implications for the history of rifting in Baffin Bay. Palynology, 15, 91–114.

Brenner, G.J. 1976. Middle Cretaceous floral provinces and early migrations of angiosperms. In: C. B. Beck (ed.), Origin and early evolution of angiosperms, Colombia University Press, New York, 23–47.

Brinkhuis, H., 1994. Late Eocene to Early Oligocene dinoflagellate cysts from the Priabonian type-area (Northeast Italy): biostratigraphy and paleoenvironmental interpretation. Palaeogeography, Palaeoclimatology, Palaeoecology, 107, 121–163.

Brinkhuis, H., Zachariasse, W.J., 1988. Dinoflagellate cysts, sea level changes and planktonic foraminifers across the Cretaceous/Tertiary boundary at El Haria, northwest Tunisia. Marine Micropaleontology, 13, 153–191.

Čech, S., Hradecká, L., Svobodová, M., Švábenická, L., 2005. Cenomanian and Cenomanian-Turonian boundary in the southern part of the Bohemian Cretaceous Basin, Czech Republic. Bulletin of Geosciences, 80, 321–354.

Courtinat, B., Crumiere, J.P., Mdon, H. and Schaaf, A., 1991. Les associations de kystes de dinoflagelles du Cenomanien-Turonien de Vergons I Bassin Vocontien France). Geobios, 24(6), 649–666.

Davey. R. J. 1969. Non-calcareous microplankton from the Cenomanian of England, northern France and North America. Part I. Bulletin of the British Museum (Natural History) Geolog, 17, 103–180.

Davey, R.J., 1969. Some dinoflagellate cysts from the Upper Cretaceous of northern Natal, South Africa. Palaeontologia Africana, 12, 1–23.

Davey, R.J., Verdier, J.P., 1973. An investigation of microplankton assemblages from latest Albian (Vraconian) sediments. Revista Española de Micropaleontologia, 5, 173–212.

Deaf, A.S., 2009. Palynology, palynofacies and hydrocarbon potential of the Cretaceous rocks of northern Egypt, University of Southampton, School of Ocean and Earth Sciences, published PhD Thesis, 348 pp.

Deflandre, G., Cookson, I.C., 1955. Fossil microplankton from Australian Late Mesozoic and Tertiary sediments. Australian Journal of Marine Freshwater Research, 6, 242–313.

Doyle, J.A., Jardiné, S., Doerenkamp, A., 1982. *Afropollis*, a new genus of early angiosperm pollen, with notes on the Cretaceous palynostratigraphy and paleoenvironments of northern Gondwana. Bulletin des Centres de Recherches Exploration-Production Elf-Aquitaine, 6, 39–117.

Ducreux, J.L., Gaillard, M.G., 1986. The Middle Cenomanian of the Saint-Laurent-de-Carnols (Gard) Lignite palynological and sedimentological data. Paleoecological implications. Géologie de la France, 189–196.

Egyptian General Petroleum Corporation (EGPC), 1996. Gulf of Suez Oilfields (A Comprehensive Overview), 688 pp.

El Beialy, S.Y., 1994a. Palynostratigraphy and palynofacies analysis of some subsurface Cretaceous Formations in the Badr el Dein (Bed 1-1) borehole, North Western Desert, Egypt. Neues Jahrbuch für Geologie und Paläontologie Abhandlungen, 192, 133–149.

El Beialy, S.Y., 1994b. Palynological investigations of Cretaceous sediments in the Abu E1 Gharadiq Oil Field, Western Desert, Egypt. Newsletters on Stratigraphy, 31, 71–84.

El Beialy S.Y., El Atfy, H.S., Zavada, M.S., El Khoriby, E.M., Abu-Zied, R.H., 2010. Palynological, palynofacies, paleoenvironmental and organic geochemical studies on the Upper Cretaceous succession of the GPTSW-7 well, North Western Desert, Egypt. Marine and Petroleum Geology, 27, 370–385.

El Beialy, S.Y., El-Soughier, M., Abdel Mohsen, S., El Atfy, H., 2011. Palynostratigraphy and paleoenvironmental significance of the Cretaceous succession in the Gebel Rissu-1 well, north Western Desert, Egypt. Journal of African Earth Sciences, 59, 215–226.

El Fawal, F.M., Hassan, H.F., Shehata, A.A., 2014. Depositional trends and sedimentary environments of the Cenomanian-Turonian sediments along G. Nezzazat-G. Ekma, South-West Sinai, Egypt. Journal of Applied Geology and Geophysics, 2, 27–38.

El Shamma, A.E., Arafa, A.A., 1992. Palynological zonation of Abu Roash "G" Member and the Upper part of Baharyia Formation in Bed Well No.1-2, Western Desert Egypt. Annals of the Geological Survey of Egypt, XVIII, 209–215.

Eshet, Y., Moshkovitz, S., Habib, D., Benjamini, C., Magaritz, M., 1992. Calcareous nannofossil and dinoflagellate stratigraphy across the Cretaceous/Tertiary boundary at Hor Hahar, Israel. Marine Micropaleontology, 18, 199–228.

Fauconnier, D., 1979. Les dinoflagelles de l'Albien et du Cenomanien inférieur du bassin de Paris. Thèse de Docteur, l'Universite d'Orleans, Doc. BGRM 5, 1–150.

Floquet, M., 1998. Outcrop cycle stratigraphy of shallow ramp deposits: The Late Cretaceous series on the Castillian Ramp (Northern Spain). In: de Graciansky, P.C., Hardenbol, J., et al. (Eds.), Mesozoic and Cenozoic Sequence Stratigraphy of European Basins. SEPM Special Publication, Tulsa, 343–360.

Foucher, J. C. 1979. Distribution stratigraphiquc des kystcs de dinoflagelles et des acritarches dans le Cretace superieur du Bassin de Paris et de]'Europe scptentrionale. Palaeontographica Abteilung B, 169, 78–105.

Ghorab, M.A., 1961. Abnormal stratigraphic features in Ras Gharib Oil Field. 3rd Arab Petroleum Congress 2, 1–10.

Haq, B.U., 2014. Cretaceous eustasy revisited. Global and Planetary Change, 113, 44–58.

Harker, S.D., Sarjeant, W.A.S., Caldwell, W.G.E., 1990. Late Cretaceous (Campanian) organic-walled microplankton from the Interior Plains of Canada, Wyoming, and Texas: biostratigraphy, palaeontology, and palaeoenvironmental interpretation. Palaeontology, 219, 1–243.

Hasenboehler, B., 1981. Etude paléobotanique et palynologique de l'Albien et du Cénomanien du Bassin Occidental Portugais au sud de l'accident de Nazaré (Province d'Estremadure), Portugal. Thèse 3ème cycle, Univ. Paris 6, 1–317.

Helby, R., Morgan, R., Partridge, A.D., 1987. A palynological zonation of the Australian Mesozoic. In: Jell, P. A. (ed.), Association of Australasian Palaeontologists, 4, 1–94.

Herngreen, G.F.W., 1973. Palynology of Albian–Cenomanian strata of borehole 1-QS-1-MA, State of Maranhao, Brazil. Pollen et Spores, 15, 515–555.

Herngreen, G.F.W., 1975. Palynology of Middle and Upper Cretaceous strata in Brazil. Mededelingen Rijks Geologische Dienst, Nieuwe Serie, 26, 39–91.

Herngreen, G.F.W., Chlonova, A.F., 1981. Cretaceous microfloral provinces. Pollen et Spores, 23, 441–556.

Herngreen, G.F.W., Kedves, M., Rovnina, L.V., Smirnova, S.B., 1996. Cretaceous palynofloral provinces: a review. In: Jansonius, J. and McGregor, D. (eds.), Palynology: principles and applications. American Association of Stratigraphic Palynologists Foundation, 3, 1157–1188.

Hochuli, P.A., 1981. North Gondwana floral elements in Lower to Middle Cretaceous sediments of southern Alps (southern Switzerland, northern Italy). Review of Palaeobotany and Palynology, 35, 337–358.

Ibrahim, M.I.A., 1996. Aptian-Turonian palynology of the Ghazalat-1 Well (GTX-1), Qattara Depression, Egypt. Review of Palaeobotany and Palynology, 94, 137–168.

Ibrahim, M.I.A., 2002. Late Albian-middle Cenomanian palynofacies and palynostratigraphy, Abu Gharadig-5 well, Western Desert, Egypt. Cretaceous Research, 23, 775–788.

Ibrahim, M.I.A., Al Hitmi, H.H.A., Kholeif, S.E., 2000. Albian-Cenomanian palynology, paleoecology and organic thermal maturity of well DK-B in the Dukhan Oil Field of Western Qatar. Arabian Journal of Geosciences, 5, 483–508.

Jardiné, S., Magloire, L., 1965. Palynologie et stratigraphie du Crétacé des bassins du Sénégal et de Côte d'Ivoire. Mémoires du Bureau de Recherches Géologiques et Minièrs, 32, 187–245.

Kedves, M., 1986. Etudes palynologiques sur les sediments préquaternaires de L`Egypt Eocene. Revista Españoła de Micropaleontologia, 18, 5–26.

Kora, M., Shahin, A., Semiet, A., 1994. Biostratigraphy and paleoecology of some Cenomanian successions in west central Sinai, Egypt. Neues Jahrbuch für Geologie und Paläontologie Monatshefte, 10, 597–617.

Kerdany, M.T., Cherif, O.H., 1990. Mesozoic. In Said, R. (ed.), The Geology of Egypt. Rotterdam, Balkema, the Netherlands, 407–438.

Lawal, O., Moullade, M., 1986. Palynological biostratigraphy of Cretaceous sediments in the Upper Benue Basin, NE Nigeria (1). Revue de Micropaléontologie, 29, 61–83.

Lister, J.K., Batten, D.J., 1988. Stratigraphic and palaeoenvironmental distribution of Early Cretaceous dinoflagellate cysts in the Hurlands farm borehole, west Sussex, England. Palaeontology, Abt. B, 210, 9–89.

Mahmoud, M.S., Moawad, A.M.M., 2000. Jurassic–Cretaceous (Bathonian to Cenomanian) palynology and stratigraphy of the West Tiba-1 borehole, northern Western Desert, Egypt. Journal of African Earth Sciences, 30, 401–416.

Mahmoud, M.S., Soliman, H.A., Deaf, A.S., 2007. Early Cretaceous (Aptian–Albian) palynology of the Kabrit-1 borehole, onshore Northern Gulf of Suez, Egypt. Revista Española de Micropaleontología, 39, 169–187.

Mansour, A., Mohamed, O., Tahoun, S.S., Elewa, A.M.T., 2018. Sequence stratigraphy of the Raha Formation, Bakr Oil Field, Gulf of Suez, Egypt: Insights from electrical well log and palynological data. Journal of African Earth Sciences, 139, 205–221.

Marshall, K.L., Batten, D.J., 1988. Dinoflagellate cyst associations in Cenomanian-Turonian "black shale" sequence of northern Europe. Review of Palaeobotany and Palynology, 54, 85–103.

Moustafa, A.G., 1976. Block Faulting in the Gulf of Suez. Proceedings of the 5th Petroleum Exploration and Production Seminar, Egypt 1, 1–19.

Muller, J., de Di Giacomo, E., van Erve, A.W., 1987. A palynological zonation for the Cretaceous, Tertiary and Quaternary of northern South America. AASP Contributions Series 19, 7–76.

Olde, K., Jarvis, I., Pearce, M., Uilčny, D., Tocher, B., Trabucho-Alexandre, J., Gröcke, D., 2015. A revised northern European Turonian (Upper Cretaceous) dinoflagellate cyst biostratigraphy: Integrating palynology and carbon isotope events. Review of Palaeobotany and Palynology, 213, 1–16.

Paterson, N.W., Mangerud, G., 2015. Late Triassic (Carnian - Rhaetian) palynology of Hopen, Svalbard. Review of Palaeobotany and Palynology, 220, 98–119.

Perry, C., Taylor, K., 2007. Environmental Sedimentology, 1st Edition, Blackwell Publishing, 441 pp.

Pavlishina, P., Wagreich, M., 2012. Biostratigraphy and paleoenvironments in a northwestern Tethyan Cenomanian-Turonian boundary section (Austria) based on palynology and calcareous nannofossils. Cretaceous Research, 38, 103–112

Pearce, M.A., Jarvis, I., Tocher, B.A., 2009. The Cenomanian-Turonian boundary event, OAE2 and palaeoenvironmental change in epicontinental seas: new insights from the dinocyst and geochemical records. Palaeogeography, Palaeoclimatology, Palaeoecology, 280, 207–234.

Peyrot, D., Barroso-Barcenilla, F., Barrón, E., Comas-Rengifo, M.J., 2011. Palaeoenvironmental analysis of CenomanianeTuronian dinocyst assemblages from the Castilian Platform (Northern-Central Spain). Cretaceous Research, 32, 504–526.

Pittet, B., Gorin, E., 1997. Distribution of sedimentary organic matter in a carbonate siliciclastic platform environment: Oxfordian deposits from the Swiss Jura Mountains. Sedimentology, 44, 915–937.

Regali, M.S.P., 1989. Tucanopollis, a new genus of early angiosperms. Boletim de Geociencias da Petrobras, 3, 395–402.

Rider, M.H., 2004. The Geological Interpretation of Well Logs, second ed. Sutherland, Scotland, 280 pp.

Salard-Cheboldaeff, M., 1990. Intertropical African palynostratigraphy from Cretaceous to Late Quaternary times. Journal of African Earth Sciences, 11, 1–24.

Schlager, W., 2005. Carbonate sedimentology and sequence stratigraphy, Oklahoma, U.S.A, 200 pp.

Schlanger, S.O., Arthur, M.A., Jenkyns, H.C., Scholle, P.A., 1987. The Cenomanian-Turonian Oceanic Anoxic Event: I. Stratigraphy and distribution of organic-rich beds and the marine d13C excursion. In: Brooks, J., Fleet, A.J. (Eds.), Marine and Petroleum Source Rocks. Geological Society London, Special Publication, 26, 371–399.

Schrank, E., 1988. Effects of chemical processing on the preservation of peridinioid dinoflagellates: a case from the Late Cretaceous of Egypt. Review of Paleobotany and Palynology, 56, 123–140.

Schrank, E., 1990. Palynology of the clastic Cretaceous sediments between Dongola and Wadi Muqaddam, northern Sudan. Berliner Geowissenschaftliche Abhandlungen, Reihe A 120, 149–168.

Schrank, E., 1992. Cretaceous correlations in Egypt and northern Sudan: palynological and paleobotanical evidence. Cretaceous Research, 13, 351–368.

Schrank, E., 1994. Nonmarine Cretaceous palynology of northern Kordofan, Sudan, with notes on fossil Salviniales (water ferns). Geologische Rundschau, 83, 773–786.

Schrank, E., 2001. Paleoecological aspects of Afropollis/Elaterates peaks (Albian- Cenomanian pollen) in the Cretaceous of northern Sudan and Egypt. In: IX International Palynological Conference, Houston, 1996, American Association of Stratigraphic Palynologists Foundation, pp. 201–210.

Schrank, E., 2003. Small acritarchs from the Upper Cretaceous: taxonomy, biological afinities and palaeoecology. Review of Palaeobotany and Palynology, 123, 199–235.

Schrank, E., Awad, M.Z., 1990. Palynological evidence for the age and depositional environment of the Cretaceous Omdurman Formation in the Khartoum area, Sudan. Berliner Geowissenschaftliche Abhandlungen, Reihe A, 120, 169–182.

Schrank, E., Mahmoud, M.S., 1998. Palynology (pollen, spores and dinoflagellates) and Cretaceous stratigraphy of the Dakhla Oasis, central Egypt. Journal of African Earth Sciences, 26, 167–193.

Schrank, E., Ibrahim, M.I.A., 1995. Cretaceous (Aptian–Maastrichtian) palynology of foraminifera-dated wells (KRM-1, AG-18) in northwestern Egypt. Berliner Geowissenschaftliche Abhandlungen, Reihe A, 177, 1–44.

Schütz, K.I., 1994. Structure and stratigraphy of the Gulf of Suez, Egypt. In: Landon, S. M. (Ed.), Interior rift basins. American Association of Petroleum Geologists Memoir, 59, 57–96.

Sultan, I.Z., Aly, S.M., 1986. Palynological zonation of Albian-Cenomanian sediments in the northern part of the Western Desert, Egypt. Bulletin of Faculty of Science, Alexandria University, 26, 80–101.

Srivastava, V., 1994. A Middle Cretaceous microfloral assemblage from Southern Coastal Tanzania. Palynology, 30, 35–48.

Tahoun, S.S., 2012. Paleoenvironmental significance of a palynomorph assemblage from the Late Albian - Cenomanian of BED 14-1 well, North Western Desert, Egypt. Egyptian Journal of Paleontology, 12, 73–95.

Tahoun, S.S., Deaf, A.S., 2016. Could the conventionally known Abu Roash "G" reservoir (upper Cenomanian) be a promising active hydrocarbon source in the extreme northwestern part of Egypt? Palynofacies, palaeoenvironmental, and organic geochemical answers. Marine and Petroleum Geology, 76, 231–245.

Tahoun, S.S., Deaf, A.S., Mansour, A., 2017. Palynological, paleoenvironmental and sequence stratigraphical analyses of a Turonian-Coniacian sequence, Beni Suef Basin, Eastern Desert, Egypt: implication of Pediastrum rhythmic signature. Marine and Petroleum Geology, 88, 871–887.

Tahoun, S.S., Ibrahim, M.I.A., Kholeif, S., 2012. Palynology and paleoenvironments of Middle Jurassic to Cenomanian successions, Alamein-IX well, north Western Desert, Egypt. Revista Española de Micropaleontologia, 44, 57–78.

Tahoun, S.S., Makled, W.A., Mostafa, T.F., 2013. Stratigraphic distribution of the palynomorphs and the particulate organic matter in subsurface Lower/Middle Cretaceous deposits, Western Desert of Egypt: Palynological and geochemical approach. Egyptian Journal of Petroleum, 22,435–449.

Tahoun, S.S., Mohamed, O., 2013. Palynology and genetic sequence stratigraphy of the reservoir rocks (Cenomanian, Bahariya Formation) in the Salam Oil Field, north Western Desert, Egypt. Cretaceous Research, 45, 342–351.

Tahoun, S.S., Mostafa, T.F., Makled, W.A., Saleh, R.A., 2015. Palynomorph biostratigraphy of the Cretaceous (Hauterivian-lower Cenomanian) of the South Sallum Well, North Western Desert, Egypt. Arabian Journal of Geosciences, 8, 9205–9219.

Thusu, B., Van der Eem, J.G.L.A., El Mehdawi, A., Bu-Argoub, F., 1988. Jurassic-Early Cretaceous palynostratigraphy in Northeast Libya. In: El Arnauti, A., Owens, B., Thusu, B. (eds.), Subsurface Palynostratigraphy of Northeast Libya, Garyounis University Publications, Benghazi, Libya, 171–213.

Tucker, M.E., 2001. Sedimentary petrology: An introduction to the origin of sedimentary rocks, Blackwell Sci. Ltd (3rd edition), USA, 272 p.

Tyson, R.V., 1989. Late Jurassic palynofacies trends, Piper and Kimmeridge Clay Formations, UK onshore and northern North Sea. In: Batten, D.J., Keen, M.C. (eds.), Northwest European Micropalaeontology and Palynology. Halsted Press, New York, 135–172.

Tyson, R.V., 1993. Palynofacies analysis. In: Jenkins, D.J. (ed.), Applied Micropalaeontology. Kluwer Academic Publishers, Dordrecht, 153-191.

Tyson, R.V., 1995. Sedimentary organic matter-organic facies and palynofacies. Chapman and Hall, London, 615 pp.

Vallati, P., 2001. Middle Cretaceous microflora from the Huincul Formation ("Dinosaurian Beds") in the Neuquén Basin, Patagonia. Argentina. Palynology, 25, 179–197.

Wood, G.D., Gabriel, A.M., Lawson, J.C., 1996. Chapter 3. Palynological techniques-processing and microscopy. In: Jansonius, J., and McGregor, D.C. (Eds.), Palynology: principles and applications. American Association of Stratigraphic Palynologists Foundation, 29–50.

Yi, S., Batten, D.J., Yun, H., Park, S.J., 2003. Cretaceous and Cenozoic non-marine deposits of the Northern South Yellow Sea Basin, offshore western Korea. palynostratigraphy and palaeoenvironments. Paleogeography, Paleoclimatology, Palaeoecology, 191, 15–44.

Received: 12 02 2018
Accepted: 26 06 2018

Omar MOHAMED[1)*)], Ahmed MANSOUR[1)], Sameh S. TAHOUN[2)], Ashraf M.T. ELEWA[1)] & Muhammad Ali MEKKEY[3)]

[1)] Geology Department, Faculty of Science, Minia University, P.O. Box 61519, Minia, Egypt;

[2)] Geology Department, Faculty of Science, Cairo University, P.O. Box 12613, Giza, Egypt;

[3)] West Bakr Petroleum Company, P.O. Box 546 Cairo-code No. 11371, Nasr City, Cairo, Egypt;

[*)] Corresponding author: omar.mohamed@mu.edu.eg

Supplementary data

Species / Sample Number		945	948	951	954	957	960	963	966	969	972	975	981	987	990	993	996	999	1002	1005	1008	1011	1014	1017	1020	1023	1026	1029	1032	1035	1038
Spores	*Cyathidites* spp.																								1						
	Cyathidites australis																		3												
	Triplanosporites spp.																		1		1										
	Concavisimisporite spp.																		2												
	Crybelosporites pannuceus														1																
	Undulatisporites spp.																														1
	Unidentified Spores																														
Gymanosperm	*Araucariacites australis*				1									4	3				8		3	1									
	Araucariacites spp.																								1						
	Ephedripites spp.													1	1																
	Inaperturopollenites spp.				1									1	3						2	3									
	Inaperturopollenites limbatus				1																										
	Cycadopites spp.			1										1								1			1						1
	Cycadopites ovatus																														
	Classopollis torosus													3	1				1												1
	Classopollis brasilensis						1							19																	
	Classopollis spp.				1				1		1			15	1				7			3			2						1
	Spheripollenites spp.								1	1				1	2										1	1					2
	Eucommiidites troedssonii													1																	
	Bisuccate pollen grain			1																											1
	Tricolporopollenites spp.													2																	
	Unidentified Pollen grains			1										1	3				2			2			1					1	1
Angiosperm	*Retimonocolpites variplicatus*																				3	1					2				
	Retimonocolpites textus																									1					
	Retimonocolpites spp.								2						1						2	1									
	Foveotricolpites giganteus													2																	
	Afropollis jardinus																				2										
	Monocolpopollenites spp.													4																	
	Tricolpites sagax													3																	

Appendix Table 1: Quantitative distribution of the palynomorphs categories in B-114 well.

Species / Sample Number		945	948	951	954	957	960	963	966	969	972	975	981	987	990	993	996	999	1002	1005	1008	1011	1014	1017	1020	1023	1026	1029	1032	1035	1038
Dinoflagellate cysts	*Spiniferites* spp.			1					2										1												
	Spiniferites ramosus														2																
	Cyclonephelium compactum								1			1		2					3	1	6	1									
	Cyclonephelium distinctum			2					2	2		1		6	4				3		2	1			1						
	Heterosphaeridium spinaconjunctum													10	2				8												
	Heterosphaeridium cordiforme			2					2	2	2	3	1	32	7			1	12		4	3									
	Pierceites cheimgoviensis										1				1						1										
	Trichodinium castanea	1		3					6	4	5	3	1	12	8			2	11	2	3	5									
	Florentinia spp.									1				2					1		1										
	Florentinia deanei													5	3				2												
	Florentinia laciniata																					1									
	Florentinia aculeata																		2												
	Isabelidinium acum-inatum													1	1																
	Oligosphaeridium spp.													1																	
	Coronifera oceanica										1			1								1									
	Acanthaulax willsonii																		4												
	Hystrichosphaeridium tubiferum																				1										
	Surculosphaeridium cf. basifurcatum																			1											
	Exochosphaeridium bifidium																		1												
	Unidentified Dinoflagellate			2					4	3	3	3	1	10	9				7	3	5	3									
F.W.A.	*Pediasstrum* spp.						2			2													1								
	Botryococcus spp.																							1						1	
Achritarchs	*Lophosphaeridium* spp.			1					1		2								2												
	Undefined Achritarchs									1	1				1																
Foraminiferal Test Linings				3			4		1		1			1					1												

Appendix Table 1: Continued.

	Species / Sample Number	987	990	993	996	999	1002	1005	1008	1011	1014	1017	1020	1023
Spores	*Cyathidites australis*									2				
	Balmeiosporites spp.									1				
	Deltoidospora spp.									1				
	Verrucosisporites major									1				
	Verrucosisporites sp.													1
	Concavisimisporite sp.									1				
	Crybelosporites pannuceus						1			15	2			2
	Crybelosporites spp.									3				
	Undulatisporites spp.									21				
	Impardecispora apiverrucatta									2				
	Pilosisporites spp.									7				
	Unidentified Spores			1				1		2				
Gymanosperm	*Araucariacites australis*		2	5	2	1		2		5				4
	Araucariacites hungaricus			1										
	Araucariacites spp.	1		1				1		4				
	Inaperturopollenites spp.	1	1					1		10				1
	Cycadopites spp.									7	1			3
	Cycadopites ovatus								1	5				
	Classopollis torosus			1							1			1
	Classopollis sp.			2	1		1	3	1	22	1			5
	Spheripollenites spp.	3	2	4	2	2	1	4	2	10	2		1	5
	Eucommiidites troedssonii													
	Exesipollenites spp.	1		1						2	1			
	Circulina spp.									2				1
	Callialasporites spp.									2				1
	Bisuccate pollen grain							2		3	2			
	Unidentified Pollen grains		2	3			2	3	3	27	3		1	6
Angiosperms	*Nyssapollenites* spp.													1
	Retimonocolpites variplicatus							1		15				
	Retimonocolpites spp.									22				
	Foveotricolpites gigantoreticulatus									9				2
	Foveotricolpites giganteus								2	3				
	Afropollis jardinus				1					1				1
	Afropollis spp.									3				
	Tricolpites spp.									3				3
	Tricolpites vulgaris									2				
	Arecipites punctatus									2				
	Arecipites spp.									5				
	Monocolpopollenites spp.		1	1					1	5				4
	Clavataspora irregularia		1					1		3				2
	Liliacidites spp.													1

Appendix Table 2: Quantitative distribution of the palynomorphs categories in B-115 well.

Species / Sample Number		987	990	993	996	999	1002	1005	1008	1011	1014	1017	1020	1023
Dinoflagellate Cysts	*Spiniferites ramosus granosus*							1						
	Spiniferites ramosus							3						1
	Cyclonephelium compactum			1				3						1
	Cyclonephelium distinctum		1	1				3		1				3
	Heterosphaeridium cordiforme					1		3		1				9
	Heterosphaeridium spp.									1			1	
	Hystrichosphaeridium recurvatum				1									
	Hystrichosphaeridium pulchrum									1				
	Disphaeria aff. hypoflata													1
	Trichodinium castanea									1				
	Florentinia spp.			2										1
	Florentinia laciniata													1
	Florentinia aculeata			1										
	Coronifera oceanica		1											2
	Systematophora cretacea		1					2						
	Systematophora aff. cretacea							2						1
	Cleistosphaeridium sp							1						
	Cleistosphaeridium armatum													1
	Exochosphaeridium bifidium							2						2
	Pyxidinopsis fairhavenesis									1				
	Unidentified Dinoflagellate		1		1				1	1			1	3
F.W.A.	*Chomotriletes minor*													
	Ovoidites parvus			1										
	Pediasstrum boryanum				2	1				1	3			5
	Pediasstrum spp.	1	1		1	1								7
Achritarchs	*Lophosphaeridium* spp.			2	1			2	1	1				3
	Unidentified Achritarchs		1	2				2		6				
Foraminiferal Test Linings		5	2	22		1	2	5					1	33

Appendix Table 2: Continued.

	Species / Sample Number	876	879	882	885	888	891	894	897	900	903	906	909	915	918	966	972	975
Spores	*Cyathidites minor*		3			1		3		2	6							
	Cyathidites spp.	1					2		1		1	2			1			1
	Cyathidites australis		2		1	9	5		2	1	3							
	Triplanosporites spp.		2			4	1		2	3	1	1						
	Deltoidospora spp.					3	1	1	1	1	14	6						
	Deltoidospora diaphana											1						
	Concavisimisporites spp.					1						1						
	Concavisimisporites punctatus									1	2							
	Clavatisporites spp.								1		1							
	Microfoveolatosporites skottsbergii				1	1		1	3		1							
	Laevigatosporites ovatus								3			1						
	Crybelosporites pannuceus													1	1			
	Crybelosporites spp.							1	3									
	Undulatisporites spp.									1								
	Biretisporites potoniaei											1						
	Biretisporites spp.		1	2					1	1	3	4						
	Punctatisporites spp.				1		1											
	Todisporites minor		1															
	Todisporites major		1						1									
	Todisporites sp.	1																
	Duplexisporites spp.						1											
	Duplexisporites generalis									1								
	Gabonisporis spp.						1											
	Cicatricosisporites spp.							1										
	Murspora cf. florida											1						
	Unidentified Spores		2	1		2	3	3	4	5	6	3						

Appendix Table 3: Quantitative distribution of the palynomorphs categories in B-109 well.

	Species / Sample Number	876	879	882	885	888	891	894	897	900	903	906	909	915	918	966	972	975
Gymanosperm	*Araucariacites australis*	4	10		4	11	2	5	16	17	12	12			1			1
	Araucariacites hungaricus	3				2	1	1	3	5	2	5						
	Araucariacites spp.					5	2	2	6	7	11	5					2	1
	Araucariacites cf. australis										1							
	Ephedripites spp.		1				1	1	1	4	3							
	Inaperturopollenites dubis		2						3	2	1	1						
	Inaperturopollenites spp.	2			2	1	2		4	6	1	11					1	1
	Inaperturopollenites undulatus				1	2			1	1	1	2						
	Inaperturopollenites giganteus								1									
	Inaperturopollenites limbatus						1											
	Cycadopites spp.		3			2	1		3	3	3	5						1
	Cycadopites ovatus											1						
	Classopollis torosus		2		1	3			1	1	1	2						
	Classopollis cf. classoides					1												
	Classopollis classoides								5									
	Classopollis tetrad											1						
	Classopollis brasilensis		2	2	1	1												
	Classopollis spp.	5				5	4	2	4	15	13	16		1	1		2	1
	Spheripollenites psilatus									1								
	Spheripollenites spp.	5	12	2	3	6	4		6	16	11	10		2	1			
	Eucommiidites troedssonii					1	1			1		2						
	Exesipollenites spp.	3	5			1	1	1	1	6	5	3		1			1	1
	Balmeioposis limbatus		1	1			1	1		2	2							
	Monosulcites spp.											1						
	Circulina spp.					2		1	1	5		1						
	Callialasporites discoidalis						1											
	Galecornea causa											1						
	Bisuccate pollen grain							1										
	Unidentified Pollen grains	5	4	4		11	1	5	16	20	10	10		2				

Appendix Table 3: Continued.

	Species / Sample Number	876	879	882	885	888	891	894	897	900	903	906	909	915	918	966	972	975
Angiosperm	*Triporites* sp.	1				1		1	1	1								
	Nyssapollenites spp.								2		2	1						
	Nyssapollenites cf. triangulus								1			1						
	Tricolporopollenites spp.	1	1				2			7	6							
	Tricolporopollenites villensis								1		1							
	Retimonocolpites variplicatus					1			2	1	2							
	Retimonocolpites spp.					1		1	1	2	1							
	Foveotricolpites gigantoreticulatus		4	1		1				1	5	6						
	Foveotricolpites aff. F. gigantoreticulatus		3		1	4	1		1	3	2	2						
	Stellatopollis densiornatus					1			2									
	Foveotricolpites giganteus		3						1	1	2							
	Foveotricolpites cf. giganteus								1									
	Foveomonocolpites spp.		1					1			2	1						
	Stellatopollis dejaxii										1							
	Afropollis jardinus											1		1	1			
	Afropollis spp.				1		1		1	1								
	Tricolpites spp.	2	3	1	1	1	2			6	11	4						
	Tricolpites sagax		1	1		1	1		2			1						
	Tetracolpites sp.						1			1	1							
	Arecipites punctatus	1	3	2								1						
	Arecipites microfoveolatus	1	1															
	Arecipites spp.		1	1		1	3		1	3	3	2						
	Rousea spp.					1					2							
	Rousea delicipollis									1								
	Monocolpopollenites spp.	4	6		1	7	1	2	10	11	11	7						
	Clavataspora irregularia		1			2	1		3	1								
	Liliacidites spp.											1						
	Liliacidites farafraensis		1															

Appendix Table 3: Continued.

	Species / Sample Number	876	879	882	885	888	891	894	897	900	903	906	909	915	918	966	972	975
Dinoflagellate cysts	*Spiniferites* spp.		1															
	Spiniferites ramosus				1	1												
	Cyclonephelium compactum		3		1			1			1	1						
	Cyclonephelium spp.					1	1			2								
	Cyclonephelium distinctum		1	1			3			1	1	1						
	Heterosphaeridium cordiforme		2	1	2		2		3	1	1							
	Heterosphaeridium spp.								1									
	Senoniasphaera spp.						1	1										
	Trichodinium castanea				2	1	1		3		1	3		1				
	Florentinia spp.		1															
	Isabelidinium acuminatum	2									2							
	Isabelidinium spp.							2										
	Isabelidinium cooksoniae									1								
	Tenua hystrix			1					1									
	Areoligera coronata							1										
	Impagidinium maghribensis								1									
	Pyxidinopsis fairhavenensis											1						
	Exochosphaeridium bifidium											1						
	Raetiaedinium truncigerum											1						
	Batiacasphaera? reticulata											1						
	Unidentified Dinoflagellate		8	1	2	5	1	2	5	6	2	2		2				1
F.W.A.	*Ovoidites parvus*		2			1	2			1	1	2						
	Ovoidites spp.							2										
	Pediasstrum boryanum				1				1									
	Pediasstrum spp.		1	1	1													1
	Scenedesmus bifidus			1														
	Chomotriletes minor	1																
Achritarchs	*Lophosphaeridium* spp.	2	3					1	1		2	2						
	Unidentified Achritarchs	1	12	1	2	6		1	2	1	2	15						
	Foraminiferal Test Linings	1					2		3		2	3						

Appendix Table 3: Continued.

Age		Upper Cretaceous-Cenomanian																													
Formation		Raha Formation																													
SOM/ Sample Nomber		1038	1035	1032	1029	1026	1023	1020	1017	1014	1011	1008	1005	1002	999	996	993	990	987	981	975	972	969	966	963	960	957	954	951	948	945
Opaque	**Equidimensional (O-Eq)** Black particle from wood material. Long axis less than twice the short axis. Without internal biostructures.	235	132	54	51	86	204	142	127	58	275	304	61	211	87	211	313	216	212	196	269	111	243	93	83	123	81	63	41	298	182
	Lath (O-La) Black particle from wood material. Long axis more than twice the short axis. Without internal biostructures.	18	23	3	8	2	18	25	15	11	16	17	5	18	3	4	22	5	11	2	21	2	4	3	3	11	2	6	2	9	6
Translucent	**Wood tracheid with pits (Wp)** Brown particle from wood tracheid with visible pits.	5	11	3	8	4	0	0	3	13	0	0	0	0	0	0	8	5	0	10	0	0	6	23	30	6	3	7	24	0	0
	Wood tracheid without pits (Ww) Brown particle from wood tracheid without visible pits.	397	290	407	341	422	211	286	302	330	211	176	18	56	33	16	181	238	166	167	52	62	429	444	494	516	407	411	578	84	65
	Cuticle (Cu) Thin cellular sheets, epidermal tissue, in some case with visible stomates	8	3	11	1	7	3	4	6	8	6	9	0	3	0	0	11	0	10	24	3	0	46	8	22	28	21	25	31	7	4
	Membranes (Mb) Thin, non-cellular, transparent sheets of probable plant origin	3	6	1	2	3	5	4	6	4	0	4	0	7	0	0	5	1	1	3	0	0	14	10	1	11	5	8	9	0	0
	Fungal hyphae (Fh) Individual filaments of mycelium of vegetative phase of eumycote fungi.	7	17	25	21	17	18	6	19	14	8	5	2	0	2	2	6	8	14	15	4	0	58	31	11	29	26	36	14	13	9
AOM	**AOM** Structureless material. Color: yellow-orange-red; orange-brown; grey. Heterogeneity: homogeneous; with "speckles"; clotted; with inclusions (palynomorphs, phytoclasts, pyrite. Form: flat; irregular; angular; pelletal (**rounded eleongate/oval shape**).	298	444	411	511	406	522	545	511	555	477	482	911	642	869	771	444	538	556	583	641	797	91	78	258	211	412	414	231	561	745
	Resin Structureless particle, **hyaline**, homogeneous, non-fluorescent, **rounded**, sharp to diffuse outline.	33	76	92	59	51	22	8	11	11	6	3	0	13	9	0	13	1	15	0	11	8	94	319	97	68	45	29	56	29	0
Spores		1	0	0	0	0	0	1	0	0	0	1	0	6	0	0	0	1	0	0	0	0	0	0	0	0	0	0	0	0	0
Pollen		7	1	0	0	2	2	6	0	0	12	12	0	18	0	0	0	15	58	0	0	1	1	4	0	0	0	4	3	0	2
Dinocysts		0	0	0	0	0	0	1	0	0	15	23	7	55	3	0	0	38	82	3	11	11	12	17	0	1	0	0	10	0	1
Acritarch		0	0	0	0	0	0	0	0	0	0	0	0	2	0	0	0	1	0	0	0	3	1	0	0	0	0	0	1	0	0
Foraminifera test Linning		0	0	0	0	0	0	0	0	0	0	0	0	1	0	0	0	0	1	0	0	1	0	1	0	0	0	0	3	0	0
Fresh Water Algea		0	1	0	0	0	0	0	1	1	0	0	0	0	0	0	0	0	0	0	0	0	2	0	0	0	0	0	0	0	0
Total		1012	1004	1007	1002	1000	1005	1028	1001	1005	1026	1036	1004	1032	1006	1004	1003	1067	1126	1003	1012	996	1001	1031	999	1004	1002	1003	1003	1001	1014

Appendix Table 4: Quantitative distribution of the palynofacies categories in B-114 well.

Age																															
Formation																															
SOM/ Sample Nomber		1038A	1035A	1032B	1029B	1026A	1023B	1020A	1017B	1014B	1011A	1008A	1005A	1002A	999B	996A	993B	990B	987A	981A	975A	972A	969A	966A	963A	960B	957A	954B	951B	948A	945A
Opaque	**Equidimen-sional (O-Eq)** Black particle from wood material. Long axis less than twice the short axis. Without internal bio-structures.	23.2	13.1	5.36	5.09	8.6	20.3	13.8	12.7	5.77	26.8	29.3	6.08	20.4	8.65	21	31.2	20.2	18.8	19.5	26.6	11.1	24.3	9.02	8.31	12.3	8.08	6.28	4.09	29.8	17.9
	Lath (O-La) Black particle from wood material. Long axis more than twice the short axis. Without internal bio-structures.	1.78	2.29	0.3	0.8	0.2	1.79	2.43	1.5	1.09	1.56	1.64	0.5	1.74	0.3	0.4	2.19	0.47	0.98	0.2	2.08	0.2	0.4	0.29	0.3	1.1	0.2	0.6	0.2	0.9	0.59
Opaque		25.0	15.4	5.7	5.9	8.8	22.1	16.2	14.2	6.9	28.4	31.0	6.6	22.2	8.9	21.4	33.4	20.7	19.8	19.7	28.7	11.3	24.7	9.3	8.6	13.3	8.3	6.9	4.3	30.7	18.5
Translucent	**Wood tracheid with pits (Wp)** Brown particle from wood tracheid with visible pits.	0.49	1.1	0.3	0.8	0.4	0	0	0.3	1.29	0	0	0	0	0	0	0.8	0.47	0	1	0	0	0.6	2.23	3	0..6	0.3	0.7	2.39	0	0
	Wood tracheid without pits (Ww) Brown particle from wood tracheid without visible pits.	39.2	28.9	40.4	34	42.2	21	27.8	30.2	32.8	20.6	17	1.79	5.43	3.28	1.59	18	22.3	14.7	16.7	5.14	6.22	42.9	43.1	49.4	51.4	40.6	41	57.6	8.39	6.41
	Cuticle (Cu) Thin cellular sheets, epider-mal tissue, in some case with visible stomates	0.79	0.3	1.09	0.1	0.7	0.3	0.39	0.6	0.8	0.58	0.87	0	0.29	0	0	1.1	0	0.89	2.39	0.3	0	4.6	0.78	2.2	2.79	2.1	2.49	3.09	0.7	0.39
	Membranes (Mb) Thin, non-cellular, transparent sheets of probable plant origin	0.3	0.6	0.1	0.2	0.3	0.5	0.39	0.6	0.4	0	0.39	0	0.68	0	0	0.5	0.09	0.09	0.3	0	0	1.4	0.97	0.1	1.1	0.5	0.8	0.9	0	0
	Fungal hyphae (Fh) Individual filaments of mycelium of vegetative phase of eumy-cote fungi.	0.69	1.69	2.48	2.1	1.7	1.79	0.58	1.9	1.39	0.78	0.48	0.2	0	0.2	0.2	0.6	0.75	1.24	1.5	0.4	0	5.79	3.01	1.1	2.89	2.59	3.59	1.4	1.3	0.89
Translucent		41.5	32.6	44.4	37.2	45.3	23.6	29.2	33.6	36.7	21.9	18.7	1.99	6.4	3.48	1.79	21	23.6	17	21.8	5.83	6.22	55.2	50	55.9	58.8	46.1	48.6	65.4	10.4	7.69

Appendix Table 4: Continued.

Phytoclasts		66.5	48.0	50.0	43.1	54.1	45.7	45.4	47.8	43.6	50.3	49.7	8.6	28.6	12.4	23.2	54.4	44.3	36.8	41.6	34.5	17.6	79.9	59.4	64.5	72.1	54.4	55.4	69.7	41.1	26.2
AOM	**AOM** Structure-less material. Color: yellow-orange-red; orange-brown; grey. Heterogeneity: homogeneous; with "speckles"; clotted; with inclusions (palynomorphs, phytoclasts, pyrite. Form: flat; irregular; angular; pelletal (**rounded eleongate/ oval shape**).	29.4	44.2	40.8	51	40.6	51.9	53	51	55.2	46.5	46.5	90.7	62.2	86.4	76.8	44.3	50.4	49.4	58.1	63.3	80	9.09	7.57	25.8	21	41.1	41.3	23	56	73.5
	Resin Structureless particle, hyaline, homogeneous, non-fluorescent, **rounded**, sharp to diffuse outline.	3.26	7.57	9.14	5.89	5.1	2.19	0.78	1.1	1.09	0.58	0.29	0	1.26	0.89	0	1.3	0.09	1.33	0	1.09	0.8	9.39	30.9	9.71	6.77	4.49	2.89	5.58	2.9	0
AOM		32.7	51.8	50.0	56.9	45.7	54.1	53.8	52.1	56.3	47.1	46.8	90.7	63.5	87.3	76.8	45.6	50.5	50.7	58.1	64.4	80.8	18.5	38.5	35.5	27.8	45.6	44.2	28.6	58.9	73.5
Spores		0.1	0	0	0	0	0	0.1	0	0	0	0.1	0	0.58	0	0	0	0.09	0	0	0	0	0	0	0	0	0	0	0	0	0
Pollen		0.69	0.1	0	0	0.2	0.2	0.58	0	0	1.17	1.16	0	1.74	0	0	0	1.41	5.15	0	0	0.1	0.1	0.39	0	0	0	0.4	0.3	0	0.2
Dinocysts		0	0	0	0	0	0	0.1	0	0	1.46	2.22	0.7	5.33	0.3	0	0	3.56	7.28	0.3	1.09	1.1	1.2	1.65	0	0.1	0	0	1	0	0.1
Acritarch		0	0	0	0	0	0	0	0	0	0	0	0	0.19	0	0	0	0.09	0	0	0	0.3	0.1	0	0	0	0	0	0.1	0	0
Foramin-ifera test Linning		0	0	0	0	0	0	0	0	0	0	0	0	0.1	0	0	0	0	0.09	0	0	0.1	0	0.1	0	0	0	0	0.3	0	0
Fresh Water Algea		0	0.1	0	0	0	0	0	0.1	0.1	0	0	0	0	0	0	0	0	0	0	0	0	0.2	0	0	0	0	0	0	0	0
Palyno-morphs		0.8	0.2	0.0	0.0	0.2	0.2	0.8	0.1	0.1	2.6	3.5	0.7	7.9	0.3	0.0	0.0	5.2	12.5	0.3	1.1	1.6	1.6	2.1	0.0	0.1	0.0	0.4	1.7	0.0	0.3
Total		100.0	100.0	100.0	100.0	100.0	100.0	100.0	100.0	100.0	100.0	100.0	100.0	100.0	100.0	100.0	100.0	100.0	100.0	100.0	100.0	100.0	100.0	100.0	100.0	100.0	100.0	100.0	100.0	100.0	100.0

Appendix Table 4: Continued.

66.5	48.0	50.0	43.1	54.1	45.7	45.4	47.8	43.6	50.3	49.7	8.6	28.6	12.4	23.2	54.4	44.3	36.8	41.6	34.5	17.6	79.9	59.4	64.5	72.1	54.4	55.4	69.7	41.1	26.2	**Phytoclasts**
32.7	51.8	50.0	56.9	45.7	54.1	53.8	52.1	56.3	47.1	46.8	90.7	63.5	87.3	76.8	45.6	50.5	50.7	58.1	64.4	80.8	18.5	38.5	35.5	27.8	45.6	44.2	28.6	58.9	73.5	**AOM**
0.8	0.2	0.0	0.0	0.2	0.2	0.8	0.1	0.1	2.6	3.5	0.7	7.9	0.3	0.0	0.0	5.2	12.5	0.3	1.1	1.6	1.6	2.1	0.0	0.1	0.0	0.4	1.7	0.0	0.3	**Palynomorphs**
1038A	**1035A**	**1032B**	**1029B**	**1026A**	**1023B**	**1020A**	**1017B**	**1014B**	**1011A**	**1008A**	**1005A**	**1002A**	**999B**	**996A**	**993B**	**990B**	**987A**	**981A**	**975A**	**972A**	**969A**	**966A**	**963A**	**960B**	**957A**	**954B**	**951B**	**948A**	945A	

Appendix Table 4: Continued.

	Phytoclasts	AOM	Palynomorphs	Microplankton	Spore	Pollen
1038A	67.0	33.0	0.8	0	1	7
1035A	48.1	51.9	0.2	0	0	1
1032B	50.0	50.0	0.0	0	0	0
1029B	43.1	56.9	0.0	0	0	0
1026A	54.1	45.7	0.2	0	0	2
1023B	45.7	54.1	0.2	0	0	2
1020A	45.5	53.9	0.8	1	1	6
1017B	47.4	51.8	0.1	0	0	0
1014B	43.3	56.0	0.1	0	0	0
1011A	50.0	46.8	2.6	15	0	12
1008A	49.5	46.6	3.5	23	1	12
1005A	8.6	90.6	0.7	7	0	0
1002A	28.5	63.3	7.9	58	6	18
999B	12.4	87.0	0.3	3	0	0
996A	23.2	76.8	0.0	0	0	0
993B	54.3	45.4	0.0	0	0	0
990B	44.2	50.4	5.2	39	1	15
987A	36.7	50.6	12.5	83	0	58
981A	41.3	57.7	0.3	3	0	0
975A	34.2	63.9	1.1	11	0	0
972A	17.5	80.5	1.6	15	0	1
969A	79.6	18.4	1.6	13	0	1
966A	59.1	38.4	2.1	18	0	4
963A	64.2	35.4	0.0	0	0	0
960B	72.1	27.8	0.1	1	0	0
957A	54.4	45.6	0.0	0	0	0
954B	55.4	44.2	0.4	0	0	4
951B	69.7	28.6	1.7	14	0	3
948A	41.1	58.9	0.0	0	0	0
945A	26.2	73.5	0.3	1	0	2

Appendix Table 4: Continued.

Age		Lower-Middle Cenomanian												
Formation		Raha Formation												
SOM/ Sample Nomber		987A	990B	993A	996A	999B	1002A	1005B	1008A	1011A	1014A	1017B	1020C	1023B
Opaque	**Equidimensional (O-Eq)** Black particle from wood material. Long axis less than twice the short axis. Without internal biostructures.	9.73	6.33	3.12	32.3	44.9	24.3	30.1	51.1	27.6	29.2	9.01	20	18.9
	Lath (O-La) Black particle from wood material. Long axis more than twice the short axis. Without internal biostructures.	6.92	0.69	0.29	1.59	1.01	2.58	1.73	2.4	3.3	1.25	0.1	0.6	0.54
Opaque		16.6	7.02	3.41	33.9	45.9	26.9	31.8	53.5	30.9	30.4	9.11	20.6	19.4
Translucent	**Wood tracheid with pits (Wp)** Brown particle from wood tracheid with visible pits.	0	0	0	0	0	0	0.2	0	0	0	0	0.1	0
	Wood tracheid without pits (Ww) Brown particle from wood tracheid without visible pits.	1.1	1.38	0.39	6.56	0	0.1	4.88	2.4	5.23	1.25	0	2.4	9.9
	Cuticle (Cu) Thin cellular sheets, epidermal tissue, in some case with visible stomates	0	0	0.2	0	0	0	0.3	0.1	0	0	0	0.8	1.52
	Membranes (Mb) Thin, non-cellular, transparent sheets of probable plant origin	0	0	0	0	0	0	0	0.2	0	0	0	0	0.36
	Fungal hyphae (Fh) Individual filaments of mycelium of vegetative phase of eumycote fungi.	0.9	0.1	1.07	0.3	0.55	0.3	0.61	0.3	0.08	0.39	1.1	1.1	0.71
Translucent		2.0	1.48	1.66	6.86	0.55	0.4	6	3	5.31	1.64	1.1	4.4	12.5
Phytoclasts		18.7	8.5	5.1	40.8	46.5	27.3	37.8	56.5	36.2	32.1	10.2	25.0	31.9
AOM	**AOM** Structureless material. Color: yellow-orange-red; orange-brown; grey. Heterogeneity: homogeneous; with "speckles"; clotted; with inclusions (palynomorphs, phytoclasts, pyrite. Form: flat; irregular; angular; pelletal (**rounded eleongate/oval shape**).	80	89.5	89.2	57.5	52.9	71.8	56.4	41.6	43.2	65.9	89.8	74.2	57.5
	Resin Structureless particle, hyaline, homogeneous, non-fluorescent, **rounded**, sharp to diffuse outline.	0.1	0.3	0.59	0.3	0	0.2	0.81	0.7	0.96	0.48	0	0.3	0
AOM		80.1	89.8	89.8	57.8	52.9	72.0	57.2	42.3	44.2	66.4	89.8	74.5	57.5
Spores		0	0	0.1	0	0	0.1	0.1	0	4.66	0.19	0	0	0.36
Pollen		0.6	0.89	1.95	0.89	0.28	0.4	1.93	1	13.7	1.06	0	0.2	3.57
Dinocysts		0	0.4	0.49	0.2	0.09	0	2.03	0.1	0.56	0	0	0.2	2.32
Acritarch		0	0.1	0.39	0.1	0	0	0.41	0.1	0.56	0	0	0	0.27
Foraminifera test Linning		0.5	0.2	2.15	0	0.09	0.2	0.51	0	0	0	0	0.1	2.94
Fresh Water Algae		0.1	0.1	0.1	0.3	0.18	0	0	0	0.08	0.29	0	0	1.07
Palynomorphs		1.2	1.7	5.2	1.5	0.6	0.7	5.0	1.2	19.6	1.5	0.0	0.5	10.5
Total		100.0	100.0	100.0	100.0	100.0	100.0	100.0	100.0	100.0	100.0	100.0	100.0	100.0

Appendix Table 5: Quantitative distribution of the palynofacies categories in B-115 well.

Age		Upper Cretaceous-Cenomanian																
Formation		Raha Formation																
SOM/ Sample Number		975	972	966	918	915	909	906	903	900	897	894	891	888	885	882	879	876
Opaque	**Equidimensional (O-Eq)** Black particle from wood material. Long axis less than twice the short axis. Without internal biostructures.	207	223	303	317	18	360	133	58	84	93	302	111	154	76	113	127	93
	Lath (O-La) Black particle from wood material. Long axis more than twice the short axis. Without internal biostructures.	14	4	17	1	1	10	4	9	3	15	33	1	9	1	7	11	20
Translucent	**Wood tracheid with pits (Wp)** Brown particle from wood tracheid with visible pits.	0	1	0	0	0	5	0	7	0	0	0	1	3	0	0	2	0
	Wood tracheid without pits (Ww) Brown particle from wood tracheid without visible pits.	148	178	323	117	45	156	124	135	197	143	187	169	178	111	42	66	54
	Cuticle (Cu) Thin cellular sheets, epidermal tissue, in some case with visible stomates	28	9	34	34	28	35	33	39	25	14	8	33	11	8	4	9	4
	Membranes (Mb) Thin, non-cellular, transparent sheets of probable plant origin	3	1	3	0	2	3	0	0	4	2	2	2	2	3	3	2	0
	Fungal hyphae (Fh) Individual filaments of mycelium of vegetative phase of eumycote fungi.	8	7	20	11	7	8	1	2	18	6	12	6	8	0	16	2	4
AOM	**AOM** Structureless material. Color: yellow-orange-red; orange-brown; grey. Heterogeneity: homogeneous; with "speckles"; clotted; with inclusions (palynomorphs, phytoclasts, pyrite. Form: flat; irregular; angular; pelletal (**rounded eleongate/oval shape**).	578	556	301	511	880	430	705	755	667	724	461	668	627	796	819	779	828
	Resin Structureless particle, **hyaline**, homogeneous, non-fluorescent, **rounded**, sharp to diffuse outline.	7	19	1	11	8	3	5	14	3	2	4	6	7	3	4	2	3
Spores		1	0	0	2	0	0	22	37	17	19	9	16	21	2	3	14	2
Pollen		6	6	0	4	6	0	115	130	151	106	26	35	76	17	15	71	37
Dinocysts		1	0	0	0	3	0	9	8	11	14	7	9	8	9	6	16	2
Achritach		0	0	0	0	0	0	17	4	1	3	2	0	6	2	1	15	3
Foraminifera test Linning		0	0	0	0	0	0	3	2	0	3	0	2	0	0	0	0	1
Fresh Water Algae		1	0	0	0	0	0	2	1	1	1	2	2	1	2	1	3	1
Total		1002	1004	1002	1008	998	1010	1173	1201	1182	1145	1055	1061	1111	1030	1034	1119	1052

Appendix Table 6: Quantitative distribution of the palynofacies categories in B-109 well.

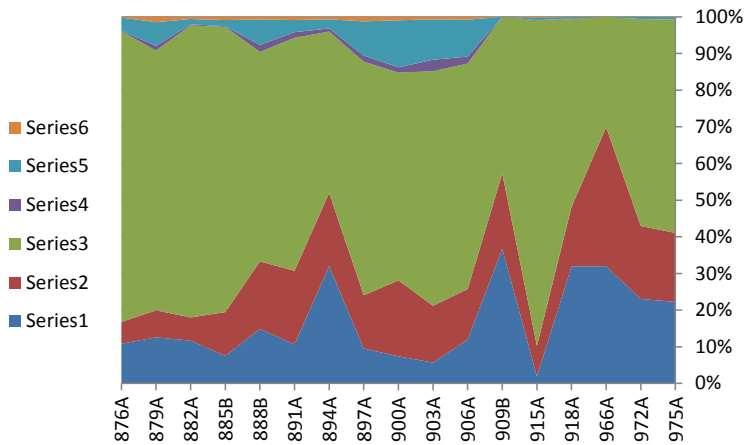

Age		Cenomanian																
Formation		Raha Formation																
SOM/ Sample Nomber		975A	972A	966A	918A	915A	909B	906A	903A	900A	897A	894A	891A	888B	885B	882A	879A	876A
Opaque	**Equidimensional (O-Eq)** Black particle from wood material. Long axis less than twice the short axis. Without internal biostructures.	20.7	22.2	30.2	31.4	1.8	35.6	11.3	4.83	7.11	8.12	28.6	10.5	13.9	7.38	10.9	11.3	8.84
	Lath (O-La) Black particle from wood material. Long axis more than twice the short axis. Without internal biostructures.	1.4	0.4	1.7	0.1	0.1	0.99	0.34	0.75	0.25	1.31	3.13	0.09	0.81	0.1	0.68	0.98	1.9
Opaque		22.1	22.6	31.9	31.5	1.9	36.6	11.7	5.6	7.4	9.4	31.8	10.6	14.7	7.5	11.6	12.3	10.7
Translucent	**Wood tracheid with pits (Wp)** Brown particle from wood tracheid with visible pits.	0	0.1	0	0	0	0.5	0	0.58	0	0	0	0.09	0.27	0	0	0.18	0
	Wood tracheid without pits (Ww) Brown particle from wood tracheid without visible pits.	14.8	17.7	32.2	11.6	4.51	15.4	10.6	11.2	16.7	12.5	17.7	15.9	16	10.8	4.06	5.9	5.13
	Cuticle (Cu) Thin cellular sheets, epidermal tissue, in some case with visible stomates	2.79	0.9	3.39	3.37	2.81	3.47	2.81	3.25	2.12	1.22	0.76	3.11	0.99	0.78	0.39	0.8	0.38
	Membranes (Mb) Thin, non-cellular, transparent sheets of probable plant origin	0.3	0.1	0.3	0	0.2	0.3	0	0	0.34	0.17	0.19	0.19	0.18	0.29	0.29	0.18	0
	Fungal hyphae (Fh) Individual filaments of mycelium of vegetative phase of eumycote fungi.	0.8	0.7	2	1.09	0.7	0.79	0.09	0.17	1.52	0.52	1.14	0.57	0.72	0	1.55	0.18	0.38
Translucent		18.7	19.5	37.9	16.1	8.22	20.5	13.5	15.2	20.6	14.4	19.8	19.9	18.2	11.8	6.29	7.24	5.89
Phytoclasts		40.7	42.1	69.9	47.6	10.1	57.1	25.1	20.8	28.0	23.8	51.6	30.4	32.9	19.3	17.9	19.6	16.6
AOM	**AOM** Structureless material. Color: yellow-orange-red; orange-brown; grey. Heterogeneity: homogeneous; with "speckles"; clotted; with inclusions (palynomorphs, phytoclasts, pyrite. Form: flat; irregular; angular; pelletal (**rounded eleongate/ oval shape**).	57.7	55.4	30	50.7	88.2	42.6	60.1	62.9	56.4	63.2	43.7	63	56.4	77.3	79.2	69.6	78.7
	Resin Structureless particle, **hyaline**, homogeneous, non-fluorescent, **rounded**, sharp to diffuse outline.	0.7	1.89	0.1	1.09	0.8	0.3	0.43	1.17	0.25	0.17	0.38	0.57	0.63	0.29	0.39	0.18	0.29
AOM		58.4	57.3	30.1	51.8	89.0	42.9	60.5	64.0	56.7	63.4	44.1	63.5	57.1	77.6	79.6	69.8	79.0
Spores		0.1	0	0	0.2	0	0	1.88	3.08	1.44	1.66	0.85	1.51	1.89	0.19	0.29	1.25	0.19
Pollen		0.6	0.6	0	0.4	0.6	0	9.8	10.8	12.8	9.26	2.46	3.3	6.84	1.65	1.45	6.34	3.52
Dinocysts		0.1	0	0	0	0.3	0	0.77	0.67	0.93	1.22	0.66	0.85	0.72	0.87	0.58	1.43	0.19
Acritarch		0	0	0	0	0	0	1.45	0.33	0.08	0.26	0.19	0	0.54	0.19	0.1	1.34	0.29
Foraminifera test Linning		0	0	0	0	0	0	0.26	0.17	0	0.26	0	0.19	0	0	0	0	0.1
Fresh Water Algae		0.1	0	0	0	0	0	0.17	0.08	0.08	0.09	0.19	0.19	0.09	0.19	0.1	0.27	0.1
Palynomorphs		0.9	0.6	0.0	0.6	0.9	0.0	14.3	15.2	15.3	12.8	4.4	6.0	10.1	3.1	2.5	10.6	4.4
Total		100.0	100.0	100.0	100.0	100.0	100.0	100.0	100.0	100.0	100.0	100.0	100.0	100.0	100.0	100.0	100.0	100.0

Appendix Table 6: Continued.

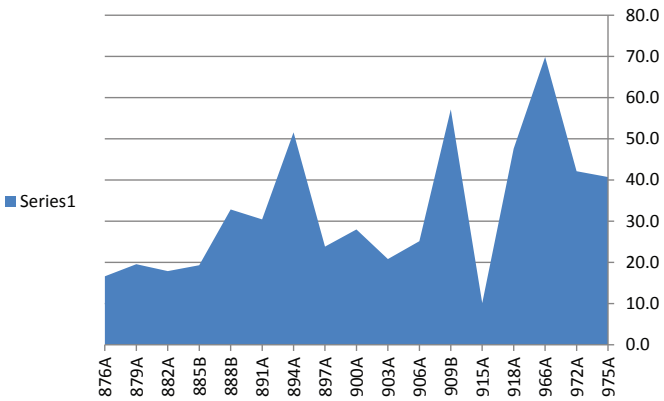

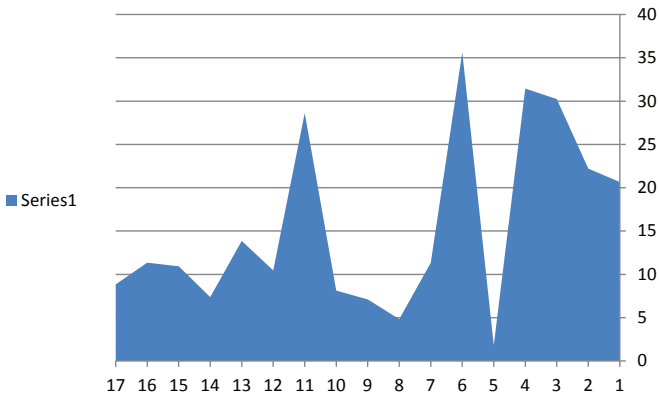

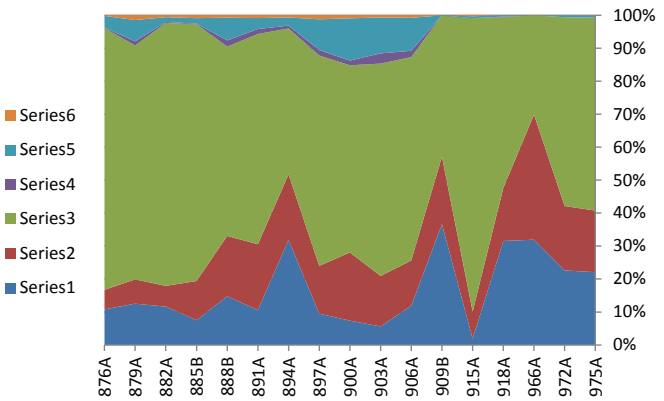

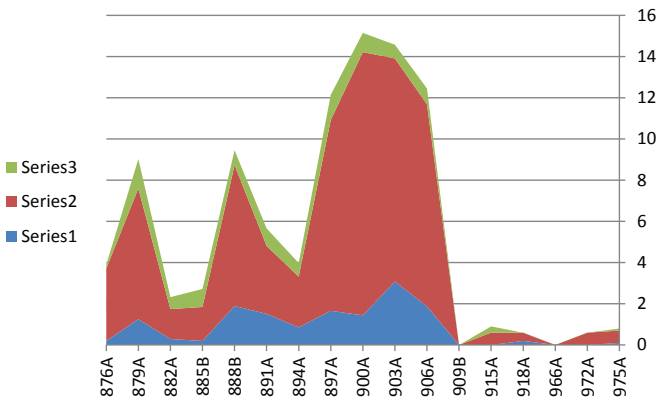

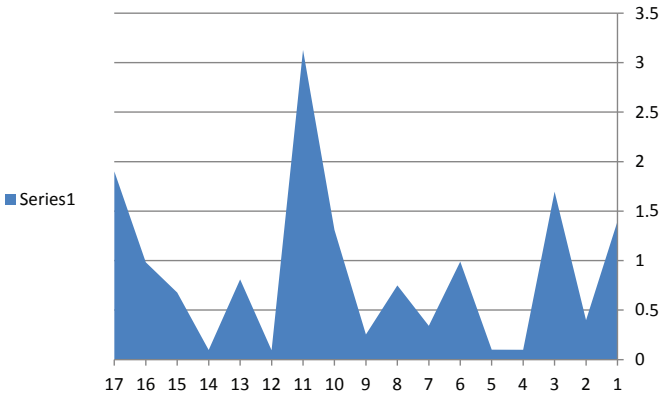

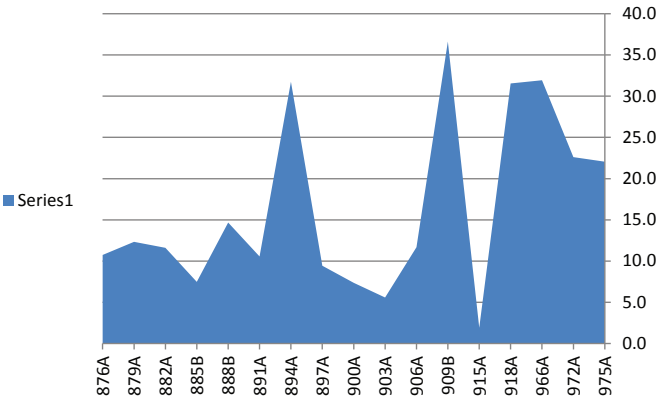

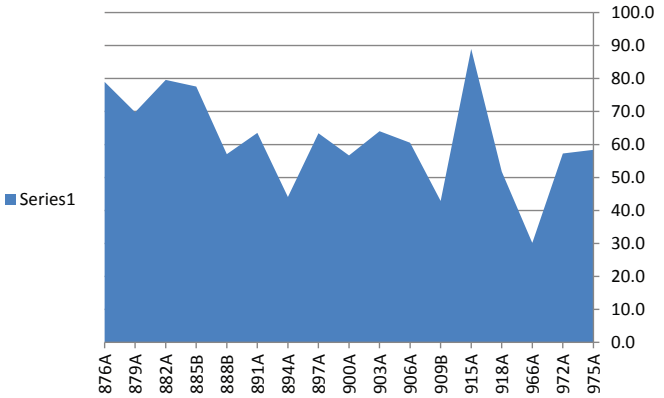

40.7	42.1	69.9	47.9	10.1	57.1	25.1	20.8	28.0	23.8	51.6	30.4	32.9	19.3	17.9	19.6	16.6	Phytoclasts
58.4	57.3	30.1	52.1	89.0	42.9	60.5	64.0	56.7	63.4	44.1	63.5	57.1	77.6	79.6	69.8	79.0	AOM
0.9	0.6	0.0	0.0	0.9	0.0	14.3	15.2	15.3	12.8	4.4	6.0	10.1	3.1	2.5	10.6	4.4	Palynomorphs
975A	**972A**	**966A**	**918A**	**915A**	**909B**	**906A**	**903A**	**900A**	**897A**	**894A**	**891A**	**888B**	**885B**	**882A**	**879A**	**876A**	
1	0	0	0	0	0	29	17	4	9	3	13	13	2	0	5	2	Spres
6	7	0	4	6	3	176	150	111	61	25	26	63	17	18	85	39	Pollen
1	0	0	0	3	0	36	22	19	17	5	8	17	9	4	22	7	Microplankton

Appendix Table 6: Continued.

	Phytoclasts	AOM	Palynomorphs	Microplankton	Spores	Pollen
975A	40.7	58.4	0.9	1	1	6
972A	42.1	57.3	0.6	0	0	6
966A	69.9	30.1	0.0	0	0	0
918A	47.9	52.1	0.0	0	0	0
915A	10.1	89.0	0.9	3	0	6
909B	57.1	42.9	0.0	0	0	0
906A	25.1	60.5	14.3	29	22	115
903A	20.8	64.0	15.2	14	37	130
900A	28.0	56.7	15.3	12	17	151
897A	23.8	63.4	12.8	20	19	106
894A	51.6	44.1	4.4	9	9	26
891A	30.4	63.5	6.0	11	16	35
888B	32.9	57.1	10.1	14	21	76
885B	19.3	77.6	3.1	11	2	17
882A	17.9	79.6	2.5	7	3	15
879A	19.6	69.8	10.6	31	14	71
876A	16.6	79.0	4.4	6	2	37

Appendix Table 6: Continued.

Age																		
Formation		Raha Formation																
SOM/ Sample Number		975A	972A	966A	918A	915A	909B	906A	903A	900A	897A	894A	891A	888B	885B	882A	879A	876A
Opaque	**Equidimensional (O-Eq)** Black particle from wood material. Long axis less than twice the short axis. Without internal biostructures.	207	223	303	317	18	360	133	58	84	93	302	111	154	76	113	127	93
	Lath (O-La) Black particle from wood material. Long axis more than twice the short axis. Without internal biostructures.	14	4	17	1	1	10	4	9	3	15	33	1	9	1	7	11	20
Translucent	**Wood tracheid with pits (Wp)** Brown particle from wood tracheid with visible pits.		1				5		7				1	3			2	
	Wood tracheid without pits (Ww) Brown particle from wood tracheid without visible pits.	148	178	323	117	45	156	124	135	197	143	187	169	178	111	42	66	54
	Cuticle (Cu) Thin cellular sheets, epidermal tissue, in some case with visible stomates	28	9	34	34	28	35	33	39	25	14	8	33	11	8	4	9	4
	Membranes (Mb) Thin, non-cellular, transparent sheets of probable plant origin	3	1	3		2	3			4	2	2	2	2	3	3	2	
	Fungal hyphae (Fh) Individual filaments of mycelium of vegetative phase of eumycote fungi.	8	7	20	11	7	8	1	2	18	6	12	6	8		16	2	4
AOM	**AOM** Structureless material. Color: yellow-orange-red; orange-brown; grey. Heterogeneity: homogeneous; with "speckles"; clotted; with inclusions (palynomorphs, phytoclasts, pyrite. Form: flat; irregular; angular; pelletal (**rounded eleongate/oval shape**).	578	556	301	511	880	430	705	755	667	724	461	668	627	796	819	779	828
	Resin Structureless particle, **hyaline**, homogeneous, non-fluorescent, **rounded**, sharp to diffuse outline.	7	19	1	11	8	3	5	14	3	2	4	6	7	3	4	2	3
Spores		1						29	17	4	9	3	13	13	2		5	2
Pollen		6	7		4	6	3	176	150	111	61	25	26	63	17	18	85	39
Dinocysts		1				3		4	1	3	1	2	3	4		3	14	3
Zooclast																		
Achritach								31	19	16	14	3	3	13	8	1	8	3
Foraminifera test Linning								1	2		2		2		1			1
Fresh Water Algae		1						3			2		1	2	2	1	1	1
Total		1002	1005	1002	1006	998	1013	1249	1208	1135	1088	1042	1045	1094	1028	1031	1113	1055

Appendix Table 6: Continued.

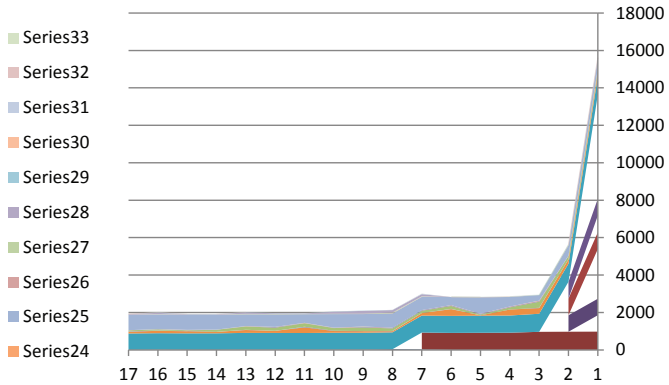

Age																		
Formation		Raha Formation																
SOM/ Sample Nomber		975A	972A	966A	918A	915A	909B	906A	903A	900A	897A	894A	891A	888B	885B	882A	879A	876A
Opaque	**Equidimensional (O-Eq)** Black particle from wood material. Long axis less than twice the short axis. Without internal biostructures.	20.66	22.21	30.24	31.45	1.804	35.64	11.34	4.829	7.107	8.122	28.63	10.46	13.861	7.379	10.928	11.35	8.84
	Lath (O-La) Black particle from wood material. Long axis more than twice the short axis. Without internal biostructures.	1.397	0.398	1.697	0.099	0.1	0.99	0.341	0.749	0.254	1.31	3.128	0.094	0.8101	0.097	0.677	0.983	1.9
Opaque		22.1	22.6	31.9	31.5	1.9	36.6	11.7	5.6	7.4	9.4	31.8	10.6	14.7	7.5	11.6	12.3	10.7
Translucent	**Wood tracheid with pits (Wp)** Brown particle from wood tracheid with visible pits.	0	0.1	0	0	0	0.495	0	0.583	0	0	0	0.094	0.27	0	0	0.179	0
	Wood tracheid without pits (Ww) Brown particle from wood tracheid without visible pits.	14.77	17.73	32.24	11.61	4.509	15.45	10.57	11.24	16.67	12.49	17.73	15.93	16.022	10.78	4.0619	5.898	5.13
	Cuticle (Cu) Thin cellular sheets, epidermal tissue, in some case with visible stomates	2.794	0.896	3.393	3.373	2.806	3.465	2.813	3.247	2.115	1.223	0.758	3.11	0.9901	0.777	0.3868	0.804	0.38
	Membranes (Mb) Thin, non-cellular, transparent sheets of probable plant origin	0.299	0.1	0.299	0	0.2	0.297	0	0	0.338	0.175	0.19	0.189	0.18	0.291	0.2901	0.179	0
	Fungal hyphae (Fh) Individual filaments of mycelium of vegetative phase of eumycote fungi.	0.798	0.697	1.996	1.091	0.701	0.792	0.085	0.167	1.523	0.524	1.137	0.566	0.7201	0	1.5474	0.179	0.38
Translucent		18.66	19.52	37.92	16.07	8.216	20.5	13.47	15.24	20.64	14.41	19.81	19.89	18.182	11.84	6.2863	7.239	5.89
Phytoclasts		40.7	42.1	69.9	47.6	10.1	57.1	25.1	20.8	28.0	23.8	51.6	30.4	32.9	19.3	17.9	19.6	16.6
AOM	**AOM** Structureless material. Color: yellow-orange-red; orange-brown; grey. Heterogeneity: homogeneous; with "speckles"; clotted; with inclusions (palynomorphs, phytoclasts, pyrite. Form: flat; irregular; angular; pelletal (**rounded eleongate/oval shape**).	57.68	55.38	30.04	50.69	88.18	42.57	60.1	62.86	56.43	63.23	43.7	62.96	56.436	77.28	79.207	69.62	78.7
	Resin Structureless particle, **hyaline**, homogeneous, non-fluorescent, **rounded**, sharp to diffuse outline.	0.699	1.892	0.1	1.091	0.802	0.297	0.426	1.166	0.254	0.175	0.379	0.566	0.6301	0.291	0.3868	0.179	0.29
AOM		58.4	57.3	30.1	51.8	89.0	42.9	60.5	64.0	56.7	63.4	44.1	63.5	57.1	77.6	79.6	69.8	79.0
Spores		0.1	0	0	0	0	0	1.876	3.081	1.438	1.659	0.853	1.508	1.8902	0.194	0	1.251	0.19
Pollen		0.599	0.598	0	0.397	0.601	0	9.804	10.82	12.77	9.258	2.464	3.299	6.8407	1.65	1.4507	6.345	3.52
Dinocysts		0.1	0	0	0	0.301	0	0.767	0.666	0.931	1.223	0.664	0.848	0.7201	0	0.5803	1.43	0.19
Acritarch		0	0	0	0	0	0	1.449	0.333	0.085	0.262	0.19	0	0.5401	0.194	0.0967	1.34	0.29
Foraminifera test Linning		0	0	0	0	0	0	0.256	0.167	0	0.262	0	0.189	0	0	0	0	0.1
Fresh Water Algae		0.1	0	0	0	0	0	0.171	0	0	0.087	0	0.189	0.09	0.194	0.0967	0.268	0.1
Palynomorphs		0.9	0.6	0.0	0.4	0.9	0.0	14.3	15.1	15.2	12.8	4.2	6.0	10.1	2.2	2.2	10.6	4.4
Total		100.0	100.0	100.0	99.8	100.0	100.0	100.0	99.9	99.9	100.0	99.8	100.0	100.0	99.1	99.7	100.0	100.0

Appendix Table 6: Continued.